Studies on photo-generation of charge carriers and their role in photoelectrochemical water splitting in few metal oxides based novel nano-hetero-structures

SYNOPSIS

Submitted in the partial fulfilment for the requirement of

Doctor of Philosophy
in
Chemistry

Submitted by
Runjhun Dutta

Under the Supervision of

Dr. Manju Srivastava
Assistant Professor
(Co-Supervisor)

Prof. Rohit Shrivastav
(Supervisor)

Department of Chemistry, Faculty of Science
Dayalbagh Educational Institute (Deemed to be University)
Dayalbagh, Agra-282005

2022

1. Solar water splitting in photoelectrochemical cell

1.1. Importance of the proposed work

Global energy demand is estimated to be doubled by 2050 **[1]** due to population expansion and rapid industrialization leading an urge to shift away from conventional energy sources **[2]**. This is also necessary for climate change mitigation, sustainable energy production and for a cleaner & greener environment **[3-8]**. Currently, it is being fulfilled largely (~81%) by fossil fuels **[9, 10]** which are depleting at a rapid rate and also contributing to the climate change and greenhouse effect **[11-13].** Development of renewable energy sources **[14]** is being simulated to avoid the future and present energy crisis and prevent environmental deterioration. Thus, the production of clean renewable energy which is storable, eco-friendly and inexpensive has become an imperative task to meet the worldwide energy demand. In order to realize these aims, scientific community is actively looking for Intermittent Renewable Energy Sources (IRES; e.g., wind, tidal power and nuclear energy etc.) **[15-20]**. Unfortunately, all these IRES suffers from some or the other drawback, for instance, low energy density, high setup cost, storage problem etc. **[21-22]**. Running these routes for energy production is also not very economical as can be inferred by analysing unit energy cost.

The search for finding an environment friendly energy source which is sustainable and pollution-free can be met by opting hydrogen as it overcomes most of the challenges faced by other fuels. For example, it possesses high energy density of 120–142 MJ kg^{-1}, which is about three times than that of gasoline. It is the cleanest available fuel, as the by-product obtained upon combustion is H_2O **[23-28]**.

Hydrogen energy actually refers to the chemical energy stored in bond of hydrogen gas, which upon splitting into atoms releases energy. This released energy can be further converted to electricity via hydrogen fuel cells **[29-31]**. Thus, hydrogen is considered as an energy carrier or a type of secondary energy source.

The production of hydrogen fuel is an essential step for the development of hydrogen energy because it is not available freely as a fuel in nature. Thus, world over scientists is working to induce a shift towards hydrogen economy **[32-33]**. Currently, the major route (50%) for hydrogen production involves steam methane reforming process which releases green-house gases **[34-35]**. Other commercial methods include refining of petroleum (30%) **[36]**, coal (18%) **[37]**, water electrolysis (4%) **[38-40]**, pyrolysis

[41, 42]. These technologies are also responsible for increasing the level of greenhouse gases. According to statistics, the global production of hydrogen in 2018 was calculated 63 million tons, which consumed ~2.2×10^8 kWh of electricity. Meanwhile, ~6.3×10^8 tons of CO_2 were emitted. The hydrogen thus produced always has CO impurity, which hinder its direct use in fuel cells for electricity generation **[43]**.

There is therefore a need for an environmentally friendly method for hydrogen production such as solar water splitting to produce green hydrogen. This route is inspired by natural photosynthesis and is sub-classified into electrochemical, photochemical, photoelectrochemical and thermochemical methods **[44]**. Production of hydrogen from solar water splitting contributes to solve the current serious environmental problems of greenhouse gas emission from the burning of fossil fuels, thus mitigating climate change. The idea of solar water splitting is inspired by natural photosynthesis, which perfectly utilizes the solar energy to convert CO_2 and water into glucose **[45-53]**.

Prime Minister of India, while speaking at the 3rd Re-inVest Conference in November 2020, had announced to launch a comprehensive National Hydrogen Energy Mission in 2021-22 for generating hydrogen from green power sources with a target of 175 GW of renewable energy capacity by the year 2022. Union Budget of India presented during February 2021, sanctioned additional capital infusion of 1,000 crores to Solar Energy Corporation of India and 1,500 crores to Indian Renewable Energy Development Agency **[85]**. The importance of this technology is also marked by the US Department of Energy which has set up a target to achieve the solar-to-hydrogen efficiency of 10% with durability of 5000 hours till 2018 and cost of photoelectrode system to be $5.7 per gasoline gallon equivalent (gge^{-1}) and $4.6 gge^{-1} for photo-particle systems in 2020 **[86-87]**.

This work will be focussed on photoelectrochemical (PEC) splitting of water for hydrogen generation which was first demonstrated in 1972 by Fujishima and Honda on single crystalline TiO_2 (rutile) as an anode and a Pt cathode under ultraviolet (UV) irradiation with an applied external bias **[54]**. Since then, efforts are being made to increase the efficiency of this process by finding a novel semiconductor material **[55-66]** due to its environmentally friendly nature **[67-84]**.

1.2 Brief Description of PEC Mechanism

The principle of PEC water splitting (as depicted in **Fig. 1**) involves conversion of light energy into electrical energy within a cell comprising **[88-96]** typically the following:

(a) Photoelectrodes (semiconductors with suitable band gap to absorb sunlight) on conductive substrates (for transport of charges)

(b) Counter Electrode (to complete the circuit)

(c) Electrolyte (to support reaction)

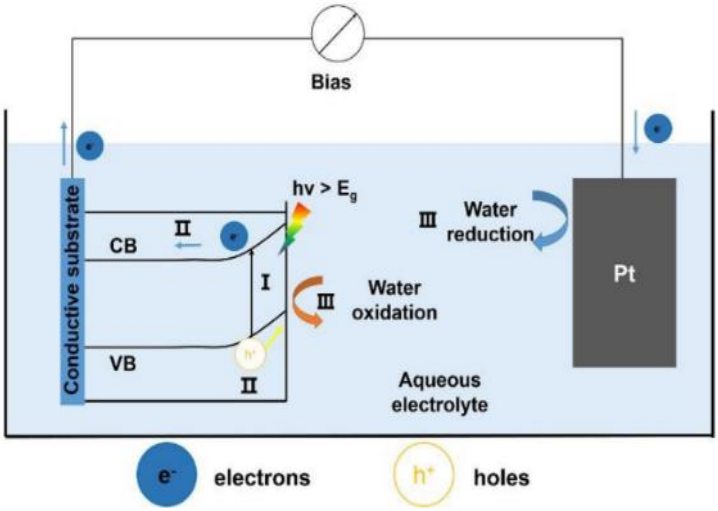

Fig. 1. Schematic diagram of a typical PEC water splitting system. Reprinted from Ref. **[97]**.

The function of semiconductor photoanode is to absorb the sun light and produce electron-hole pairs which separate due to the built-in electric field at the semiconductor electrolyte interface and the external bias. In summary, electrons move through the external circuit toward the counter electrode for HER & holes travel across the depletion layer to the semiconductor surface for OER. Thus, OER and HER occur at different locations, so that the oxygen and hydrogen could be effectively separated and collected to yield high purity products.

The overall water splitting process is depicted in the equation (1, 2 and 3), where E^0_{ox} is O_2 evolution potential [1.23 V (vs. NHE) at pH=0], E^0_{red} are H_2 evolution potential [0 V (vs. NHE) at pH=0] and ΔG^0 is the change of the Gibbs free energy before and after water-splitting reaction. **[98]**

Hydrogen evolution reaction (HER):

$$2\,H^+ + 2\,e^- \xrightarrow[hv>E_g]{} H_2\,(g) \qquad \{Eqn.01\} \qquad E^o_{red} = 0\ V$$

Oxygen evolution reaction (OER):

$$2\,H_2O \xrightarrow[hv>E_g]{} O_2(g) + 4\,H^+ + 4e^- \qquad \{Eqn.02\} \qquad E^o{}_{ox} = 1.23\ V$$

Overall reaction:

$$2\,H_2O \xrightarrow[hv>E_g]{} O_2(g) + 2H_2(g) \qquad \{Eqn.03\} \qquad \Delta E^\circ = -1.23\ V\ (\Delta G^\circ = 273.18\ kJ\ mol^{-1})$$

Corresponding to these equations, the energy of 273 kJ is required for splitting one mole of water molecule i.e., a minimum voltage of 1.23 V of potential energy is indispensable. Therefore, the absorption of light by photoelectrode must be equal to or larger than 1.23 eV of energy. In fact, there is always an estimated total energy loss of about 0.8 eV induced by overpotential due to the recombination of photogenerated electrons and holes, and voltage losses at the contacts. As a result, an external bias is still needed even if the bandgap of photoelectrode materials is larger than 1.23 eV because of the fact that the practical voltage required for PEC water splitting is approximately 2.0 eV. **[99-103]**

In summary, the basic mechanism of photoelectrochemical water splitting in general is based on the photoexcited charge carrier's generation. Generally, PEC water splitting reaction on semiconductor involves three main steps: (a) absorption of light energy exceeding the semiconductor bandgap (E_g) which generates electron (e^-) and hole (h^+) pairs inside the semiconductor; (b) these electrons and holes are separated followed by migration of charges to the interface of the semiconductor particles; (c) surface chemical reactions between these carriers typically H_2O, electrons and holes to produce H_2 and O_2. **[104-123]**.

1.3 Semiconductor requirements

Due to the above facts, there are some stringent requirements for a semiconductor material to be used as photoelectrode, such as (i) bandgap should lie in the visible light responsive range of 1.6−1.8 eV, (ii) charge carrier diffusion length must be high, (iii) chemically stable in acidic and alkaline solutions, and (iv) band edge positions should straddle between water oxidation and reduction potentials i.e. VB must be more positive than the oxidation potential of H_2O to O_2 (1.23 V vs NHE at pH=0) and CB must be more negative than the proton reduction potential of H^+ to H_2 (0 V vs NHE at pH=0). **[124-125]**

2. Motivation of the proposed work

2.1 Recombination of electron-hole pairs: A Major Challenge

One of the major challenges in PEC is of electron-hole recombination which is related to surface or interface sites, internal defects and dislocations, depletion region, built-in electric field, external bias, drifting velocity, and mean free path. All these factors significantly reduce the efficiency of converting the absorbed photons into redox reactions **[126]**. Another concern which needs to be addressed for the commercial viability of this process is of photo-corrosion leading to instability **[127-133]**. Other factors which need to be optimized **[134]** by successive characterization are summarized in **Fig. 2** for development of stable, nontoxic, cheap, and visible-light-driven photoelectrode materials.

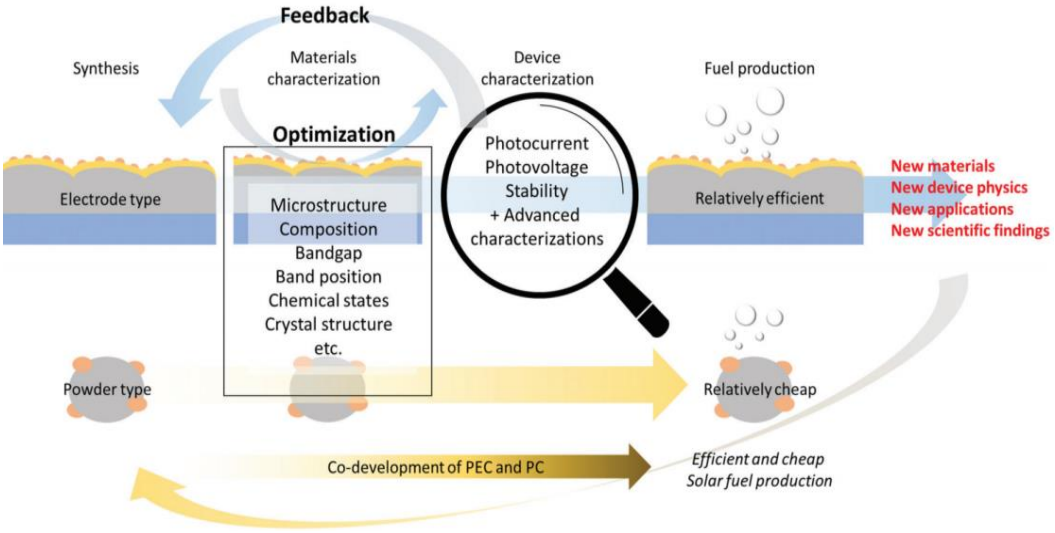

Fig. 2 Schematic illustration of various factors which needs to be optimized for PEC research. Reprinted from Ref. **[134]**.

The recombination mechanism can be briefly described as that after the separation of the photogenerated carriers, the electrons diffuse to the photoelectrode surface and reduce the protons in the water to form H_2, whereas the holes oxidize the water to form O_2. In this process, part of the e^-/h^+ pairs recombine depending on the number of carriers that can reach the photoelectrode surface, and the energy is lost in the form of heat energy **[137-139]**.

Charge recombination can be reduced by proper engineering of the electronic structures, modification of charge migration behavior, tailoring of interfacial properties, and amplification of heterostructure electromagnetic fields. It leads to efficient light harvesting, promoted charge separation and transport, and accelerated surface reactions. In short, this work will be focused on designing a semiconductor

material and judging its photo generated charge carrier behavior so as to reduce the recombination of charge carrier to the minimum. This will lead to an optimized system giving higher photocurrent density.

2.2 Investigation of charge recombination

In order to investigate the carrier dynamics of designed semiconductor material in PEC system, various techniques have been utilized, including electrochemical impedance spectroscopy (EIS), intensity-modulated photocurrent/photovoltage spectroscopy (IMPS/IMVS), time-resolved photoluminescence (TRPL) spectroscopy, transient absorption spectroscopy (TAS), and transient photocurrent/photovoltage (TPC/TPV) measurements.

Among them, EIS is the relatively widely used technique to test the electrochemical impedance of a PEC device, which implies the frequency response of PEC devices. EIS data can be inter-converted to Nyquist plots or Bode phase plots. **[140-141]**

It can be easily inferred from **Fig. 5** that the semicircle radius in a Nyquist plot is proportional to the carrier transfer impedance at the electrode/electrolyte interface, and the smaller semicircle radius implies the smaller carrier transfer impedance. The equivalent circuit model can be acquired from the impedance experimental data, and drawn as the relationship between the actual admittance and the imaginary admittance, including the series resistance, the charge-transfer resistance across the electrode/electrolyte interfaces, and the constant-phase element for electrode/electrolyte interfaces. The diameter of the circle in low frequency range is inversely proportional to the charge separation efficiency. The Bode phase plots can be utilized to estimate the electron lifetime. Thus, both the carrier transportation and recombination kinetics can be reflected by EIS technique. **[142-143]**

3. Recent Literature Survey: A summary

Planned work is majorly concerned with the introduction of metal oxides along with carbon interfaced materials such as graphene and MWCNTs. Details of literature review can be found in Annexure 1.

3.1 Metal Oxides

Easy manufacturing, high abundance, relatively high stability and tunable band edges has led to exploration of metal oxides as photoelectrodes. However, low charge separation is still a major concern in case of bare anodic oxides such as TiO_2, ZnO, SnO_2, WO_3, Fe_2O_3, and Cu_2O. Their performance highly depends on the rational design of heterostructures with engineered electronic structures, modified

charge migration behavior, tailored interfacial properties, and amplified electromagnetic fields. All these enable the achievement of efficient light harvesting, promoted charge separation and transport, and accelerated surface reactions. **[144-148]**

Development and optimization of metal oxides coupled with carbon interfaced materials such as graphene and MWCNTs is a subject of great interest today **[177-261]**. Literature has been explored in detail to study all the possible aspects of metal oxide @ carbon interfaced materials (graphene/ MWCNTs). Please refer to **Table A.1** and **Table A.2** for details.

3.2 Perovskite like Metal Oxides

Perovskite like metal oxides (ABO_3) have high activity/ durability and excellent compositional and structural flexibility, superior sunlight absorption capability and precise control of band gaps and band edges. More specifically, alkali metals (Li, Na, etc.), alkaline-earth metals (Ba, Sr, etc.) and rare-earth metals (La, Pr, etc.) can occupy the A site of perovskite oxides while a number of transition metals (Ti, Fe, Co, Mn, Ta, etc.) can be used as the B-site elements. **[149-151]**

The intrinsic conductivity of perovskite oxides can be greatly enhanced through the rational selection of A/B site elements and B-site doping with non-metal elements such as phosphorus (P) and boron (B) **[152]**. In addition, both A and B sites can be substituted by other metal cations to form $A_{1-x}A'_xBO_3$ or $AB_{1-y}B'_yO_3$. Furthermore, the adjustable bulk and surface components as well as the easy tailoring of the physical and chemical properties of perovskite oxides offer great potential to tune the photoexcitation. To further improve the PEC performance of the photoelectrode, it is important to combine multiple surface design strategies. **[153-158]**

For instance, $LaFeO_3$, a popular photoelectrode in PEC water splitting, has demonstrated potential for improved PEC response by increasing the electrical conductivity through rational selection of the compositional elements and functional dopants as well as control of the oxygen vacancy concentration. This work has been performed for preliminary analysis and has shown increment in photocurrent density relative to the pristine material. Details can be found in the section entitled “Work done so far”.

3.3 Graphene

Graphene is a crystal of carbon atoms with single atom thickness. The carbon atoms re-arranged in a honeycomb crystal lattice. By rolling up and stacking up graphene other forms of graphene can be

made, such as nanotubes and 3D crystal of graphite. Graphene has attracted much attention due to its exciting properties such as having only one atom thick, two-dimensional crystal structure, linear dispersion of quasiparticles in graphene **[159]**. There are various available forms of Graphene such as monolayer graphene **[160]**, bilayer graphene **[161]**, graphene quatum dot **[162-164]**, graphene superlattices **[165]**, graphene nanoribbons, graphene fibre, 3D graphene **[166]** and pillared graphene **[167]** etc.

The one which is majorly been explored by scientists with a combination of metal oxides is Graphene Oxide. Results showed that that graphene oxide had optical band gap of 2.5, 2.45 and 2.35 eV for acetone, deionized water and ethanol respectively. **[168]**

Graphene shows many desirable properties for a flexible transparent conductive material. Some of them are atomic thickness, high transparency and outstanding carrier mobility. **[169]** With reference too optical properties, graphene has a linear dispersion relation whereas semiconductors tend to have quadratic dispersion, which attributes to a number of desirable physical and electronic properties of graphene with atomic thickness in the range of 3 Angstrom. **[170-171]**

The electrons in graphene have very long mean free paths. Hence, graphene's properties are different from what is found in usual metals and semiconductors. Graphene has also a robust but flexible structure with unusual phonon modes that do not exist in ordinary 3D solids. Interestingly enough, these properties can be easily modified with the application of electric and magnetic fields, addition of layers, control of its geometry, and chemical doping. Moreover, graphene can be directly and relatively easily probed by various scanning probe techniques from mesoscopic down to atomic scales, because it is not buried inside a 3D structure. This makes graphene one of the most versatile systems **[172]**.

The more graphene layers there are stacked on top of each other, the greater the light absorption becomes and the lower the optical transparency becomes. But the relationship is linear, with each layer absorbing 2.3% of light; so, a graphene sample composed of 5 layers would have an absorption of 11.5 % and an optical transparency of around 88-88.5% (when you also take into account the small degree of light reflected). Graphene possesses unique optical transitions and can absorb light over a wide range of frequencies due to its band structure, lack of a band gap and the interaction between the electromagnetic radiation and the Dirac fermions in the graphene sheet. **[173-176]**

If a graphene sheet is rolled up along one axis, it forms a carbon nanotube (CNT). So, literature has been briefly looked up for the application of multi walled CNTs as a photoelectrode. Details can be found in Annexure 1.

4. Proposed work

4.1 Proposed Study

The genesis of the proposed work lies in the need to develop a greater insight on charge carrier generation and recombination and the desire to build efficient PEC systems for solar-hydrogen generation. The proposed study would be focused on the preparation and characterization of some layered/ doped chosen materials and investigates their performance in photo splitting of water. Materials of interest will be chemically stable metal oxides, perovskite and graphene based materials; absorbing largely in the UV and visible region. The main thrust of the present study would be to explore the extent to which such nanostructures/ nanoarchitectures of metal oxides get functionalized towards improved PEC response for splitting water. The broad objectives/stages of the present study have been outlined below.

4.2 Objectives/ Stages of the Proposed Work

The present study would essentially be based on photoelectrochemical investigations using layered/ core shell nanostructures/ nanoarchitectures of chosen metal oxides for photo-splitting of water. The following broad objectives will be taken into account.

(a) The preparation of layered/ core shell nanostructures /nanoarchitectures of metal oxides (thin film) by wet chemical methods (sol-gel and spray pyrolysis etc.).

(b) Sample characterization prepared for parameters mentioned in **Table** 1.

(c) Photoelectrochemical investigations (pertaining to photo-splitting of water) using samples prepared under objective (a).

Table 1: Tentative plan of the proposed work

Parameters of the study	Description
Preparation of samples • Materials of interest	Few of the following: ZnO, α-Fe_2O_3, CuO/Cu_2O, TiO_2, $LaFeO_3$, carbon interfaced material such as graphene on metal oxides etc.
Proposed Avenues for Investigation	▪ Nanostructures/Nanoarchitectures ▪ Layered structures ▪ Core Shell structures
Proposed method for the preparation of samples	Wet chemical process (Sol-gel and spray pyrolysis).
Expected variables in the study	**Preparation of samples:** ▪ Nature of metal oxides and their combinations ▪ Sintering Conditions: Temperature, Environment
Characterization	▪ Phase analysis by XRD ▪ Surface morphology by SEM ▪ Surface Topography by AFM ▪ Charge carrier dynamics by Electrochemical Impedence Spectroscopy (Nyquist Plot) ▪ Band gap energy by UV-Vis spectrophotometer ▪ Flatband potential and charge carrier density by Mott-Schottky
PEC measurement variables	▪ Current-Voltage characteristics of the PEC cell under darkness and illumination. ▪ Photovoltage & Photocurrent ▪ Open circuit potential ▪ Short Circuit current ▪ Onset voltage ▪ Applied bias photon to current conversion efficiency (ABPE)

4.3 Proposed Methodology

Thin films will be prepared by wet chemical routes using precursor solution. Films will be deposited on conducting glass substrate by spin-coating or spray pyrolysis. Samples will be subjected to high temperature sintering to evolve the crystalline phase. All the samples, thus prepared, will be characterized for structural, morphological, electrical/electronic and optical characteristics by standard methods using X-ray diffractometer, scanning electron microscope, atomic force microscope and UV-visible spectrometer. The PEC studies will be performed by using prepared samples as working electrodes (WE) in the PEC cells. Xenon Arc light source will be employed for illumination.

4.4 Expected outcome

An increased value of photocurrent density relative to the pristine material is expected with good stability of semiconductor material which may offer a cheap and efficient substitute for green / solar hydrogen generation.

5. Work Done so Far

Among all the perovskite like metal oxides, Lanthanum Iron Oxide ($LaFeO_3$) is an attractive candidate for the desired application because of its stability, environmental friendliness and the relatively high earth abundance of the constituent elements. But the kinetics of the transfer of photogenerated electrons to water needs to be enhanced as they tend to get trapped at surface states thus favoring recombination. The strategy adopted is partial change in concentration of La ions through a similar oxidation state and ionic radius which can disturb the valency of the perovskite matrix, generating oxygen vacancies, and enhancing the mobility of surface-adsorbed lattice oxygen. Because of the addition of analogous valence metal, ions disrupt the crystal matrix and improve the perovskite stability resulting in an enhanced redox performance. **[262-263]**

$LaFeO_3$ perovskites was synthesized loaded with different Tungsten (W) ion concentration through a citric sol-gel route. Physicochemical properties were systematically investigated and the impact of W ion loading on the crystal structure was optimized. The as-synthesized perovskites showed an increase in majority carrier concentration resulting from a dopant-induced increase of the Fe density caused by charge compensation upon substitution of La by W.

5.1 Experimental Details:

The method of fabrication is divided here in four different sections.

5.1.1 Preparation of precursor sol for W doped $LaFeO_3$

A citric sol-gel route is employed for the preparation of the different films using ITO conducting glass as a substrate. To synthesize the pristine $LaFeO_3$ sample, $La(NO_3)_3 \cdot 6H_2O$ (0.3 M) and $Fe(NO_3)3 \cdot 9H_2O$ (0.3 M) were dissolved in water and the solution was stirred for 1 h. Then, the appropriate amount of citric acid monohydrate was added to reach a concentration of 0.6 M and the solution was stirred again for 20 h. The $La_{1-x}FeW_xO_3$ and $LaFe_{1-x}W_xO_3$ (with x=1, 0.025, 0.075) electrodes were obtained using the above-described procedure, but substituting the corresponding amount of the La & Fe salt by

Tungstosilicic acid hydrate ($H_4[W_{12}SiO_{40}]$) according to the final desired stoichiometry. The above-mentioned solutions were mixed with acetylacetone (30 µL/mL) and Triton 100X (30 µL/mL).

5.1.2 Thin film preparation

Multilayer thin films were synthesized by uniformly coting the prepared sol on 1 x 1 cm^2 fluorine tin oxide coated glass substrate at 3000 rpm. After each successive layer, film was allowed to dry on hot plate for 10 min at 80°C. Finally, films were calcined at 600°C for 2 hours in tubular furnace. **5.1.3.**

5.1.3 Preparation of electrodes

Copper wire, silver paste and hysol was used for converting the thin films into electrode. Uncoated area of the electrode was used to give an ohmic contact with the help of copper wire and silver paste. The contact area was then covered with non-conducting and non-transparent epoxy-resin.

Three different types of electrodes opted for study are described in Table 2.

Table 2: Sample Abbreviations

Sample	Sample Code
$LaFeO_3$	P
$La_{1-x}FeW_xO_3$ (x=0.025)	P1
$La_{1-x}FeW_xO_3$ (x=0.075)	P7

5.2 Results and Discussion

Photoelectrochemical performance of thin films after converting them into photoelectrodes was done under dark and illumination conditions. station (Zahner) and Xe arc lamp (150 W). All these experiments were performed in (0.1M) NaOH electrolyte.

5.2.1 Current-Voltage Curve

Photocurrent density of the prepared P, P1, P7 was examined with the help of current-voltage graph in 0.1M NaOH. The plot of photocurrent density (PCD) versus applied potential is shown in **Fig. 3**.

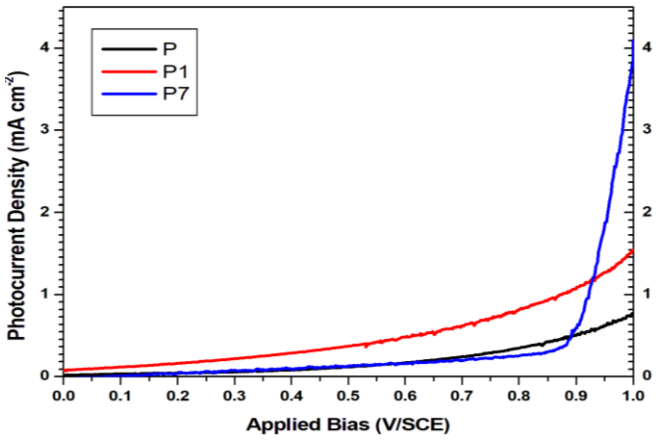

Fig. 3 Photocurrent density vs applied potential of sample P, P1 and P

It can be seen in **Fig. 3** that in pristine $LaFeO_3$, the maximum photocurrent density of 0.7 mA cm^{-2} at 0 V/SCE is obtained, whereas in W doped $LaFeO_3$, 1.5 mA cm^{-2} (P1) and 4.2 mA cm^{-2} (P7) at 0 V/SCE is obtained in the sample having two layers of deposition. This may be ascribed due to high charge storage capacity of the sample.

To justify the improvement in PEC response, various other electrochemical characterizations were also carried out and are discussed in following sections.

5.2.2 Mott-Schottky curves

Mott-Schottky analysis was also performed in order to get the information about flat band potential under dark.

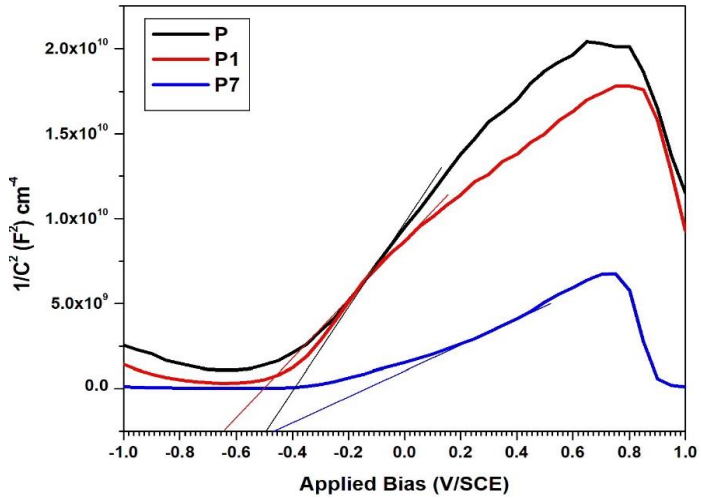

Fig. 4. Mott-Schottky plot of sample P, P1 and P7

Positive slope obtained in the curves (**Fig. 4**) confirm n-type nature of semiconductor. Flatband potential (V_{FB}) exhibited a shift from - 0.64 V/SCE in P to -0.49 V/SCE (P1) and -0.45 V/SCE (P7). This suggest

that space charge region has decreased due to the fact that more electrons are attracted towards it. Lower $1/C^2$ value of P1 and P7 in comparison to P showed that doping has led to higher capacitance of the system which may be attributed to the surface defects and high vacancy formation, thereby significantly improving the PEC performance.

5.2.3 Electrochemical impedance spectroscopy (EIS) study

Charge transfer kinetics at the electrode/electrolyte interface was studied using electrochemical impedance spectroscopy (EIS). Nyquist plot were obtained from EIS and are shown in **Fig. 5**. The plot shows that semicircular arc of the P1 and P7 is smaller as compared to P showing reduction in charge transfer resistance for sample which definitely indicates far better charge transfer properties in sample.

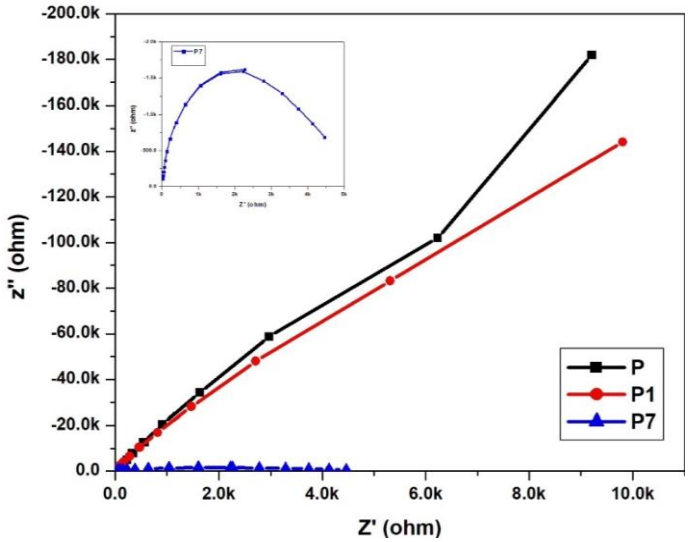

Fig. 5. Nyquist Plot of P, P1 and P7 obtained from EIS Measurements

5.3 Conclusion

Positive slope obtained in the Mott-Schottky curve confirm n-type nature of semiconductor. This slope is inversely proportional to the density of majority charge carriers. So, density of charge carriers is P7 > P1 > P. Lower $1/C^2$ value of P1 and P7 in comparison to P showed that doping has led to higher capacitance of the system which may be attributed to the surface defects and high vacancy formation. Nyquist plot shows that semicircular arc of the P1 and P7 is smaller as compared to P leading to the conclusion that there is reduction in charge transfer resistance for sample. It can be concluded that doping of W in $LaFeO_3$ has led to better charge transfer properties in the sample which has approximately doubled the photocurrent density value. Hence, improvement in PEC response as shown in Table 3 is justified by Mott Schottky and Electrochemical Impedence Spectroscopic analysis.

Table 3 : Photocurrent Density of samples

Sample Code	Sample	Current Density
P	$LaFeO_3$	0.7 mA cm^{-2}
P1	$La_{0.975}Fe_1W_{0.025}O_3$	1.5 mA cm^{-2}
P7	$La_{0.925}Fe_1W_{0.075}O_3$	4.2 mA cm^{-2}

This work has been presented as a poster in a conference and the abstract of the same entitled "Tungsten doped $LaFeO_3$: Synthesis and Photoelectrochemical measurements for water splitting" has been published as a conference proceeding in 8th Interdisciplinary Symposium on Materials Chemistry organized by Chemistry Division, Bhabha Atomic Research Centre, Mumbai-400085, India and Society for Materials Chemistry, India supported by Board of Research in Nuclear Sciences, Department of Atomic Energy, Government of India from 17 June 2021 to 19 June 2021.

REFERENCES

[1] N. S. Lewis and D. G. Nocera (2006), *Proceedings of the National Academy of Sciences of the United States of America*. 103, 15729-15735.

[2] A. Engels, M. Kunkis and S. Altstaedt, A new energy world in the making: Imaginary business futures in a dramatically changing world of decarbonized energy production, *Energy Res. Soc. Sci.*, 2020, **60**, 101321.

[3] N. Delaporte, E. Rivard, S.K. Natarajan, P. Benard, M.L. Trudeau and K. Zaghib, Synthesis and Performance of MOF-Based Non-Noble Metal Catalysts for the Oxygen Reduction Reaction in Proton-Exchange Membrane Fuel Cells: A Review, *Nanomaterials*, 2020, 10, **10**,1947.

[4] B. Lin and J. Zhu, Determinants of Renewable Energy Technological Innovation in China under CO_2 Emissions Constraint, *J. Environ. Manag*., 2019, **247**, 662–671.

[5] J. Zeng, T. Liu, R. Feiock and F. Li, The Impacts of China's Provincial Energy Policies on Major Air Pollutants: A Spatial Econometric Analysis, *Energy Policy*, 2019, **132**, 392–403.

[6] C.L. Hu, L. Zhang and J.L. Gong, Recent progress made in the mechanism comprehension and design of electrocatalysts for alkaline water splitting, *Energy Environ. Sci.*, 2019, 12, **9**, 2620-2645.

[7] M. Xiao, Z. Wang, M. Lyu, B. Luo, S. Wang, G. Liu, H.M. Cheng and L. Wang, Hollow nanostructures for photocatalysis: advantages and challenges, *Adv. Mater.*, 2019, 31, **38**, 1801369.

[8] T. Leijtens, K.A. Bush, R. Prasann and M.D. McGehee, Opportunities and challenges for tandem solar cells using metal halide perovskite semiconductors, *Nat. Energy*., 2018, 3, **10**, 828-838.

[9] *International Energy Agency in World Energy Outlook*(2011).

[10] *Key World Energy Statistics*(2013).

[11] F. E. Osterloh and B. A. Parkinson, *MRS Bulletin*, (2011), 36, 17-22.

[12] S. H. Habisreutinger, L. Schmidt-Mende and J. K. Stolarczyk (2013).*Angew. Chem*. Int. Ed. 52, 7372-7408.

[13] N. S. Lewis, and D. G. Nocera, *Proc. Natl. Acad. Sci. USA*, (2006). 103, 15729-15735.

[14] Lee, M. G., Park, J. S., & Jang, H. W. (2018). Solution-processed metal oxide thin film nanostructures for water splitting photoelectrodes: a review. *Journal of the Korean Ceramic Society*, *55*(3), 185-202.

[15] World Energy Needs and Nuclear Power|EnergyNeeds|Nuclear Energy meeting Energy Needs—World Nuclear Association. Available online: https://www.world-nuclear.org/information-library/current-andfuture-generation/world-energy-needs-and-nuclear-power.aspx.

[16] S.S. Ho and S. Kristiansen, Environmental Debates over Nuclear Energy: Media, Communication, and the Public, *Environ. Commun*., 2019, **13**, 431–439.

[17] L. Al-Ghussain, R. Samu, O. Taylan and M. Fahrioglu, Sizing Renewable Energy Systems with Energy Storage Systems in Microgrids for Maximum Cost-Efficient Utilization of Renewable Energy Resources, *Sustain. Cities Soc*., 2020, **55**, 102059.

[18] R. Dua, K. White and R. Lindland, Understanding Potential for Battery Electric Vehicle Adoption Using Large-Scale Consumer Profile Data, *Energy Rep*., 2019, **5**, 515–524.

[19] J.F. De Carolis and D.W. Keith, The real cost of wind energy, *Science*, 2001, 294, **5544**, 1000-1003.

[20] Z.L. Wang, T. Jiang and L. Xu, Toward the blue energy dream by triboelectric nanogenerator networks, *Nano Energy*, 2017, **39**, 9-23.

[21] S.S. Pang, Advances in thermochemical conversion of woody biomass to energy, fuels and chemicals, *Biotech Adv.*, 2019, 37, **4**, 589-597.

[22] E. Rivard, M. Trudeau and K. Zaghib, Hydrogen Storage for Mobility: A Review, *Materials*,2019, **12**, 1973.

[23] MIT Study: Quebec Hydro Reservoirs Provide Valuable Energy Storage for U.S. Northeast. Available online: https://www.hydroreview.com/2020/02/18/mit-study-quebec-hydro-reservoirs-providevaluable-energy-storage-for-u-s-northeast/

[24] K. T. Møller, T. R. Jensen, E. Akiba and H.-w. Li (2017).*Progress in Natural Science: Materials International*. 27, 34-40.

[25] Xiao L, Ying Wu S, Li YR. (2012) Advances in solar hydrogen production via two-step water-splitting thermochemical cycles based on metal redox reactions. *Renew. Energy*. 41:1-12.

[26] Y. Yang, S. Niu, D. Han, T. Liu, G. Wang and Y. Li (2017).*Advanced Energy Materials*. 7, 1700555.

[27] W. Si, Z.P. Tehrani, F. Haydous, N. Marzari, I.E. Castelli, D. Pergolesi and T. Lippert, Yttrium tantalum oxynitride multiphases as photoanodes for water oxidation, *J. Phys. Chem. C.*, 2019, 123, **43**, 26211-26217.

[28] A. Ali and P.K. Shen, Nonprecious metal's graphene-supported electrocatalysts for hydrogen evolution reaction: fundamentals to applications, *Carbon Energy*, 2020, 2, **1**, 99-121.

[29] X.Q. Du, C.R. Huang and X.S. Zhang, Surface modification of a Co_9S_8 nanorods with $Ni(OH)_2$ on nickel foam for high water splitting performance, *Int. J. Hydrogen Energy*, 2019, 44, **36**, 19953-19966.

[30] J.O. Abe, A.P.I. Popoola, E. Ajenifuja and O.M. Popoola, Hydrogen Energy, Economy and Storage: Review and Recommendation, *Int. J. Hydrogen Energy*, 2019, **44**, 15072–15086.

[31] X. Ren, L. Dong, D. Xu and B. Hu, Challenges towards Hydrogen Economy in China, *Int. J. Hydrogen Energy*, 2020, 45, **59**, 34326-34345.

[32] T. Sinigaglia, T.E. Freitag, F. Kreimeier and M.E.S. Martins, Use of Patents as a Tool to Map the Technological Development Involving the Hydrogen Economy, *World Pat. Inf.*, 2019, **56**, 1–8.

[33] C. Marchal, M. Behr, F. Vigneron, V. Caps and V. Keller, Au/TiO_2 photocatalysts prepared by solid grinding for artificial solar light water splitting, *New J Chem.*, 2016, 40, **5**, 4428-4435.

[34] J. Zhang, Q.Y. Zhang and X.L. Feng, Support and interface effects in water-splitting electrocatalysts, *Adv Mater.*, 2019, 31, **31**, 1808167.

[35] S. D. Angeli, G. Monteleone, A. Giaconia and A. A. Lemonidou (2014).*International Journal of Hydrogen Energy*. 39, 1979-1997.

[36] Azenha C, Lagarteira T, Mateos-Pedrero C, Mendes A (2020). Production of hydrogen from methanol steam reforming using $CuPd/ZrO_2$ catalysts- influence of the catalytic surface on methanol conversion and CO selectivity. *Int J Hydrogen Energy*.

[37] Chen Y,Wang Y, Xu H, Xiong G. (2008) Hydrogen production capacity of membrane reformer for methane steam reforming near practical working conditions. *J Membr Sci*; 322:453-9.

[38] Cai F, Lu P, Ibrahim JJ, Fu Y, Zhang J, Sun Y (2019). Investigation of the role of Nb on Pd Zn catalyst in methanol steam reforming for hydrogen production. *Int J Hydrogen Energy*. 44:11717-33.

[39] Al-Zareer M, Dincer I, Rosen MA. Production of hydrogenrich (2020).Syngas from novel processes for gasification of petroleum cokes and coals. *Int. J. Hydrogen Energy*. 45:11577-92.

[40] A. Ko¨rner, C. Tam, S. Bennett and J. Gagne´ (2015).*International Energy Agency (IEA)*, Paris, France.

[41] E. L. Miller (2015), *Energy Environ. Sci*.8, 2809 RSC.

[42] Nguyen T, Abdin Z, Holm T, Merida W (2019). Grid-connected hydrogen production via large-scale water electrolysis. *Energy Convers Manag* 2019. 200:112108.

[43] Chi J, Yu H (2018). Water electrolysis based on renewable energy for hydrogen production. *ChinJCatal*. 39: 390-4.

[44] Li W, Wei M, Liu Y, Ye Y, Li S, Yuan W, et al (201(=9). Catalysts evaluation for production of hydrogen gas and carbonnanotubes from the pyrolysis-catalysis of waste tyres. *Int J Hydrogen Energy*. 44:19563-72.

[45] L. Wang, Y. Tong, J. Feng, J. Hou, J. Li, X. Hou and J. Liang G-C_3N_4-based films: a rising star for photoelectrochemical water splitting, *Sustainable Mater. Technol.*, 2019, **19**, e00089.

[46] A. Steinfeld, Solar thermochemical production of hydrogen-a review, *Sol. Energy*, 2005, **78**, 603-15.

[47] Saidi K, Omri A (2020). Reducing CO_2 emissions in OECD countries: do renewable and nuclear energy matter? *Prog Nucl Energy*.126:103425.

[48] Watson N.D., Miller J.B., Taylor L.V., Lovell J.B., Cox J.W., Fedors J.C., Kopia L.P., Holloway R.M., Bradley O.H (1985). Earth Radiation Budget Experiment (ERBE) scanner instrument anomaly investigation. *NASA Technical memorandum* 1985.19860007082.

[49] N. S. Lewis (2007). Science. 315, 798-801.

[50] T. Hisatomi, J. Kubota and K. Domen (2014).*Chem. Soc. Rev*.43, 7520-7535.

[51] N. S. Lewis and D. G. Nocera (2006).*Proc. Natl. Acad. Sci. U. S. A*.103, 15729–15735

[52] C. Battaglia, A. Cuevas and S. De Wolf (2016). *Energy Environ. Sci*.9, 1552–1576.

[53] L. Li, Y. Zheng, S. Zhang, J. Yang, Z. Shao and Z. Guo (2018).*Energy Environ. Sci*.11, 2310–2340.

[54] G. L. Soloveichik (2015).*Chem. Rev.*115, 11533–11558.

[55] T. R. Cook, D. K. Dogutan, S. Y. Reece, Y. Surendranath, T. S. Teets and D. G. Nocera (2010).*Chem. Rev*. 110, 6474–6502.

[56] A. Fujishima and K. Honda, Electrochemical Photolysis of Water at a Semiconductor Electrode, *Nature*, 1972, **238**, 37.

[57] M. Gratzel (2001). Nature. 414, 338.

[58] Z. B. Chen, H. N. Dinh, E. Miller (2013). Photoelectrochemical Water Splitting: Standards, Experimental Methods, and Protocols, *Springer, New York.*

[59] B. A. Pinaud, J. D. Benck, L. C. Seitz, A. J. Forman, Z. B. Chen, T. G. Deutsch, B. D. James, K. N. Baum, G. N. Baum, S. Ardo, H. L. Wang, E. Miller, T. F. Jaramillo (2013).*Energy Environ*. Sci.6, 1983.

[60] M. Fang, G. F. Dong, R. J. Wei, J. C. Ho (2017).*Adv. Energy Mater*. 7, 1700559.

[61] H. L. Wu, X. B. Li, C. H. Tung, L. Z. Wu (2018). *Adv. Sci*. 2018. 5, 1700684.

[62] Tamirat, A. G., Rick, J., Dubale, A. A., Su, W. N., & Hwang, B. J. (2016). Using hematite for photoelectrochemical water splitting: a review of current progress and challenges. *Nanoscale Horizons*, *1*(4), 243-267.

[63] A. J. Bard and M. A. Fox (1995). *Acc. Chem. Res*.28, 141-145.

[64] J. Gong, C. Li and M. R. Wasielewski (2019).*Chemical Society Reviews*. 48, 1862-1864.

[65] L. Q. Wang, Y. Y. Tong, J. M. Feng, J. G. Hou, J. Li, X. G. Hou and J. Liang (2019).*Sustainable Materials and Technologies.*19,00089.

[66] Joy, J.; Mathew, J.; George, S. C (2018). Nanomaterials for Photoelectrochemical Water Splitting-Review. *Int. J. Hydrogen Energy*. 43, 4804.

[67] Li, J.; Wu, N (2015). Semiconductor-Based Photocatalysts and Photoelectrochemical Cells for Solar Fuel Generation: A Review. *Catal. Sci. Technol*. 5, 1360.

[68] Hisatomi, T.; Kubota, J.; Domen, K (2014). Recent Advances in Semiconductors for Photocatalytic and Photoelectrochemical Water Splitting. *Chem. Soc. Rev*. 43, 7520.

[69] P. H. Pfromm (2017).*J. Renewable Sustainable Energy*. 9, 034702.

[70] E. S. Andreiadis, M. Chavarot-Kerlidou, M. Fontecave, V. Artero (2011).*Photochem. Photobiol*. 87, 946.

[71] Steinfeld A (2005). Solar thermochemical production of hydrogen-a review. *Sol Energy*. 78:603-15.

[72] Z. Sun, M. Yang, Y. Wang and Y. H. Hu (2019).*ACS Applied Energy Materials*. 2, 1102-1110.

[73] M. Yang, Z. Sun and Y. H. Hu (2019).*The Journal of Physical Chemistry C*. 123, 12142-12148.

[74] X. Z. Shangcong Sun, Xianlong Liu, Lun Pan, Xiangwen Zhang, Jijun Zou (2020).*ActaPhysico-ChimicaSinica*. 36, 1905007.

[75] A. Miyoshi, S. Nishioka and K. Maeda (2018).*Chemistry – A European Journal*. 24, 18204-18219.

[76] F. Liu, C. Huang, C.-X. Liu, R. Shi and Y. Chen (2020). *Chemistry – A European Journal*. 26, 4449-4460.

[77] E. Rahmanian, R. Malekfar and M. Pumera (2018).*Chemistry – A European Journal*. 24, 18-31.

[78] B. Han and Y. H. Hu (2015).*The Journal of Physical Chemistry C*. 119, 18927-18934.

[79] S. Fang, Z. Sun and Y. H. Hu (2019).*ACS Catalysis*. 9, 5047- 5056.

[80] Z. Sun, S. Fang, Y. Lin and Y. H. Hu (2019).*Chemical Engineering Journal*. 375, 121909.

[81] S. Fang, Y. Liu, Z. Sun, J. Lang, C. Bao and Y. H. Hu (2020).*Applied Catalysis B: Environmental*. 278, 119316.

[82] B. A. Pinaud, J. D. Benck, L. C. Seitz, A. J. Forman, Z. Chen, T. G. Deutsch, B. D. James, K. N. Baum, G. N. Baum, S. Ardo, H. Wang, E. Miller and T. F. Jaramillo (2013).*Energy Environ. Sci.*6, 1983–2002.

[83] Hisatomi and K. Domen (2019).*Nat.Catal*. 2, 387–399.

[84] Reddy IN, Reddy ChV, Sreedhar A, Cho M, Kim D, Shim J (2019). Effect of plasmonic Ag nanowires on the photocatalytic activity of Cu doped Fe_2O_3 nanostructures photoanodes for superior photoelectrochemical water splitting applications. *J Electroanal Chem*. 842:146-60.

[85] Lianos P (2017). Review of recent trends in photoelectrocatalytic conversion of solar energy to electricity and hydrogen. *Appl Catal B Environ*. 210:235-54.

[86] Chen R, Zhen C, Yang Y, Sun X, Irvine JTS, Wang L, et al (2019). Boosting photoelectrochemical water splitting performance of Ta_3N_5 nanorod array photoanodes by forming a dual cocatalyst shell. *Nano Energy*. 59:683-8.

[87] Indian Budget Speech of Minister of Finance, 2021-2022. https://www.indiabudget.gov.in/doc/budgetspeech.pdf

[88] DOE, Hydrogen Production Technical Team Roadmap, 2013. http://www1.eere.energy.gov/vehiclesandfuels/pdfs/program/hpttroadmapjune2013.pdf

[89] DOE, Photoelectrochemical Hydrogen Production: DOE PEC Working Group Overview, 2011. http://www.hydrogen.energy.gov/pdfs/progress10/iig1miller.pdf

[90] D. A. Tryk, A. Fujishima and K. Honda, *Electrochim. Acta*, 2000, **45**, 2363-2376.

[91] Y. Li, J. Li, W. Yang and X. Wang, Implementation of ferroelectric materials in photocatalytic and photoelectrochemical water splitting, *Nanoscale Horiz*., 2020,5, **8**, 1174-1187.

[92] M. Grätzel, Photoelectrochemical Cells, *Nature,* 2001, **414**, 338

[93] Alfaifi B. Y., Ullah H., Alfaifi S., Tahir A. A., and Mallick T. K (2018). Photoelectrochemical solar water splitting: From basic principles to advanced devices. Veruscript Functional Nanomaterials. 2: #BDJOC3.

[94] I. Roger, M. A. Shipman and M. D. Symes (2017)*Nature Reviews Chemistry*. 1, 0003.

[95] Simrjit Singh, Hongjun Chen, Shamim Shahrokhi, Luyuan Paul Wang, Chun-Ho Lin, Long Hu, Xinwei Guan, Antonio Tricoli, Zhichuan J. Xu, and Tom Wu (2020). Hybrid Organic−Inorganic Materials and Composites for Photoelectrochemical Water Splitting.*ACS Energy Lett*. 5, 1487−1497.

[96] Yang, W., Prabhakar, R. R., Tan, J., Tilley, S. D., & Moon, J. (2019). Strategies for enhancing the photocurrent, photovoltage, and stability of photoelectrodes for photoelectrochemical water splitting. *Chemical Society Reviews*, *48*(19), 4979-5015.

[97] D. Stolten (2010) Hydrogen and fuel cells: fundamentals, technologies and applications, *John Wiley & Sons*.

[98] Kim, J. H.; Hansora, D.; Sharma, P.; Jang, J. W.; Lee, J. S. (2019). Toward Practical Solar Hydrogen Production-An Artificial Photosynthetic Leaf to-Farm Challenge. *Chem. Soc. Rev*. 48, 1908.

[99] Y. Li, J. Li, W. Yang and X. Wang, Implementation of ferroelectric materials in photocatalytic and photoelectrochemical water splitting, *Nanoscale Horiz*., 2020,5, **8**, 1174-1187

[100] Reddy, C. V., Reddy, K. R., Shetti, N. P., Shim, J., Aminabhavi, T. M., & Dionysiou, D. D. (2020). Hetero-nanostructured metal oxide-based hybrid photocatalysts for enhanced photoelectrochemical water splitting–A review. *Int. J. of hydrogen energy*, *45*(36), 18331-18347.

[101] Y. Yang, S. Niu, D. Han, T. Liu, G. Wang and Y. Li, Progress in developing metal oxide nanomaterials for photoelectrochemical water splitting, *Adv. Energy Mater*., 2017, 7, **19**, 1700555.

[102] G. Wang, Y. Ling, H. Wang, L. Xihong and Y. Li, Chemically modified nanostructures for photoelectrochemical water splitting, *J. Photochem. Photobiol. C,* 2014, **19**, 35-51.

[103] S.N. Ariffin, H.N. Lim, Z.A. Talib, A. Pandikumar and N.M. Huang. Aerosol-assisted chemical vapor deposition of metal oxide thin films for photoelectrochemical water splitting. *Int. J. Hydrogen Energy*, 2015, 40, **5**, 2115-2131.

[104] J.W. Ager, M.R. Shaner, K.A. Walczak, I.D. Sharp, S. Ardo, Experimental demonstrations of spontaneous, solar-driven photoelectrochemical water splitting, *Energy Environ. Sci*. 2015, 8, **10**, 2811-2824.

[105] D.K. Lee, D. Lee, M.A. Lumley and K.S. Choi, Progress on ternary oxide-based photoanodes for use in photoelectrochemical cells for solar water splitting, *Chem. Soc. Rev.*, 2019, 48, **7**, 2126-2157.

[106] M. R. Hoffman, S. T. Martin and W. Choi (1995).*Chem. Rev*.95, 69-96.

[107] A. L. Linsebigler, G. Q. Lu and J. T. Yates (1995).*Chem. Rev*.95, 735-758.

[108] A. Mills and S. J. Hunte, J. Photochem. Photobiol. A, 1997, 108, 1-35.

[109] A. Fujishima, X. T. Zhang and D. A. Tryk (2008).*Surf. Sci. Rep*. 63, 515-582.

[110] E. Barsoukov, J. R. Macdonald (2005). Impedance spectroscopy Theory, experimental, and Applications, *ed. 2nd Ed. John Wiley, New Jersey.*

[111] C. Zhen, R. Chen, L. Wang, G. Liu and H.-M. Cheng (2016).*Journal of Materials Chemistry A*. 4, 2783-2800.

[112] A. B. Murphy, P. R. F. Barnes, L. K. Randeniya, I. C. Plumb, I. E. Grey, M. D. Horne and J. A. Glasscock (2006).*Int. J. of Hydrogen Energy*. 31, 1999-2017.

[113] Ikeda S, Itani T, Nango K, Matsumura M (2004). Overall water splitting on tungsten-based photocatalysts with defect pyrochlore structure. *Catal Lett*. 98:229-33.

[114] Lewis NS (2001). Light work with water. *Nature.* 414:589-90.

[115] M. R. Nellist, F. A. Laskowski, F. Lin, T. J. Mills and S. W. Boettcher (2016).*Acc. Chem. Res*.49, 733–740.

[116] K. Sivula and M. Graetzel (2013). Photoelectrochemical water splitting: materials, processes and architectures, *Royal Society of Chemistry*.

[117] Peter, L. M. (2015). Photoelectrochemical water splitting. A status assessment. *Electroanalysis*, *27*(4), 864-871.

[118] Chen X., Shen S., Guo L., and Mao S. S (2010). Semiconductor-based photocatalytic hydrogen generation. *Chemical Reviews*. 110 (11): 6503–6570.

[119] Li R (2017). Latest progress in hydrogen production from solar water splitting via photocatalysis, photoelectrochemical, and photovoltaic-photoelectrochemical solutions. *Chinese Journal of Catalysis*. 38 (1): 5–12.

[120] Walter M. G., Warren E. L., McKone J. R., Boettcher S. W., Mi Q., et al. (2010). Solar water splitting cells. *Chemical Reviews*. 110 (11): 6446–6473.

[121] Navarro R. M., Alvarez-Galván M. C., Villoria de la Mano J. A., Al-Zahrani S. M., and Fierro J. L. G (2010). A framework for visible-light water splitting. *Energy and Environmental Science*. 3 (12): 1865.

[122] J.-K. G. Wei Zhou, Sheng Shen, Jinbo Pan, Jie Tang, Lang Chen, Chak-Tong Au, Shuang-Feng Yin (2020).*ActaPhysico-ChimicaSinica*. 36, 1906048.

[123] G. Xie, K. Zhang, B. Guo, Q. Liu, L. Fang and J. R. Gong (2013).*Advanced Materials*. 25, 3820-3839.

[124] S. Wang, G. Liu and L. Wang (2019).*Chemical Reviews*. 119, 5192-5247.

[125] Tamirat, A. G., Rick, J., Dubale, A. A., Su, W. N., & Hwang, B. J. (2016). Using hematite for photoelectrochemical water splitting: a review of current progress and challenges. *Nanoscale Horizons*, *1*(4), 243-267.

[126] C. Jiang, S. J. A. Moniz, A. Wang, T. Zhang and J. Tang, *Chem. Soc. Rev.*, 2017, **46**, 4645-4660.

[127] A.B. Murphy, P. R. F. Barnes, L. K. Randeniya, I. C. Plumb, I. E. Grey, M. D. Horne and J. A. Glasscock, *Int. J. Hydrogen Energy*, 2006, **31**, 1999-2017.

[128] C. Acar and I. Dincer, A Review and Evaluation of Photoelectrode Coating Materials and Methods for Photoelectrochemical Hydrogen Production, *Int. J. Hydrogen Energy*, 2016, **41**, 7950.

[129] S. Liu, L. Zheng, P. Yu, S. Han and X. Fang, Novel Composites of α Fe_2O_3 Tetrakaidecahedron and Graphene Oxide as an Effective Photoelectrode with Enhanced Photocurrent Performances, *Adv. Funct. Mater*., 2016, **26**, 3331.

[130] F.X. Xiao, J. Miao and B. Liu, Layer-by-Layer Self-Assembly of CdS Quantum Dots/Graphene Nanosheets Hybrid Films for Photoelectrochemical and Photocatalytic Applications, *J. Am. Chem. Soc.*, 2014, **136**, 1559.

[131] Y.K. Kim and H. Park, Light-Harvesting Multi-Walled Carbon Nanotubes and CdS Hybrids: Application to Photocatalytic Hydrogen Production from Water, *Energy Environ. Sci.*, 2011, **4**, 685.

[132] Y. Liu, D.P. Wang, Y.X. Yu, W.D. Zhang, Preparation and Photoelectrochemical Properties of Functional Carbon Nanotubes and Ti co-doped Fe_2O_3 Thin Films, *Int. J. Hydrogen Energy*, 2012, **37**, 9566.

[133] P. Sharma, J.W. Jang and L.S. Lee, Key strategies to advance the photoelectrochemical water splitting performance of α-Fe_2O_3 photoanode, *Chem. Cat. Chem.*, 2019, 11, **1**, 157-179.

[134] C. Li, Z. Luo, T. Wang and J. Gong, Surface, bulk, and interface: rational design of hematite architecture toward efficient photo-electrochemical water splitting, *Adv Mater.*, 2018, 30, **30**, 1707502.

[135] L. Wang, J. Han, J. Feng, X. Wang, D. Su, X. Hou, J. Hou, J. Liang and S.X. Dou, Simultaneously efficient light absorption and charge transport of CdS/TiO_2 nanotube array toward improved photoelectrochemical performance, *Int. J. Hydrogen Energy*. 2019, 44, **59**, 30899-30909.

[136] W. Yang, R. R. Prabhakar, J. Tan, S. D. Tilley and J. Moon, Strategies for enhancing the photocurrent, photovoltage, and stability of photoelectrodes for photoelectrochemical water splitting, Degradation in photoelectrochemical devices: Review with an illustrative case study, *Chem. Soc. Rev.*, 2019, 48, **19**, 4979-501.

[137] B. Yao, J. Zhang, X. Fan, J. He, Y. Li, Small 2019, 15, 1803746.

[138] X. T. Xu, L. Pan, X. Zhang, L. Wang, J. J. Zou, Adv. Sci. 2019, 6, 1801505.

[139] M. Q. Yang, J. Wang, H. Wu, G. W. Ho, Small 2018, 14, 1703323.

[140] Xu, W., Tian, W. and Li, L., 2021. Two-Dimentional Nanostructured Metal Oxide/Sulfide–Based Photoanode for Photoelectrochemical Water Splitting. *Solar RRL*, *5*(6), p.2000412.

[141] L. Wang, K. Marcus, X. Huang, Z. Shen, Y. Yang, Y. Bi, Small 2018, 14, 1704464.

[142] L. Meng, X. Zhou, S. Wang, Y. Zhou, W. Tian, P. Kidkhunthod, S. Tunmee, Y. Tang, R. Long, Y. Xin, L. Li, Angew. Chem. Int. Ed. 2019, 58, 16668.

[143] Y. Wang, W. Tian, L. Chen, F. Cao, J. Guo, L. Li, ACS Appl. Mater. Interfaces 2017, 9, 40235.

[144] Chen, Y.Z., Jiang, D.J., Gong, Z.Q., Li, J.Y. and Wang, L.N., 2020. Anodized metal oxide nanostructures for photoelectrochemical water splitting. *International Journal of Minerals, Metallurgy and Materials*, *27*(5), pp.584-601.

[145] Y. Yang, S.W. Niu, D.D. Han, T.Y. Liu, G.M. Wang, and Y. Li, Progress in developing metal oxide nanomaterials for photoelectrochemical water splitting, Adv. Energy Mater., 7(2017), No. 19, art. No. 1700555.

[146] C.V. Reddy, I.N. Reddy, K.R. Reddy, S. Jaesool, and K. Yoo, Template-free synthesis of tetragonal Co-doped ZrO2 nanoparticles for applications in electrochemical energy storage and water treatment, Electrochim. Acta, 317(2019), p. 416.

[147] C.V. Reddy, I.N. Reddy, B. Akkinepally, V.V.N. Harish, K.R. Reddy, and S. Jaesool, Mn-doped ZrO2 nanoparticles prepared by a template-free method for electrochemical energy storage and abatement of dye degradation, Ceram. Int., 45(2019), No. 12, p. 15298.

[148] Xia, C., Wang, H., Kim, J.K. and Wang, J., 2021. Rational Design of Metal Oxide-Based Heterostructure for Efficient Photocatalytic and Photoelectrochemical Systems. *Advanced Functional Materials*, *31*(12), p.2008247.

[149] W. Wang, M. O. Tade, Z. Shao, Chem. Soc. Rev. 2015, 44, 5371-5408.

[150] P. Tan, M. Liu, Z. Shao, M. Ni, Adv. Energy Mater. 2017, 7, 1602674.

[151] W. Wang, M. O. Tadé, Z. Shao, Prog. Mater. Sci. 2018, 92, 33-63

[152] Y. Zhu, W. Zhou, J. Yu, Y. Chen, M. Liu, Z. Shao, Chem. Mater. 2016, 28, 1691-1697

[153] S. Choi, S. Park, J. Shin, G. Kim, J. Mater. Chem. A 2015, 3, 6088- 6095.

[154] S. P. Jiang, L. Liu, K. P. Ong, P. Wu, J. Li, J. Pu, J. Power Sources 2008, 176, 82-89.

[155] M. Li, W. Zhou, X. Xu, Z. Zhu, J. Mater. Chem. A 2013, 1, 13632-13639.

[156] J. M. Porras-Vazquez, T. F. Kemp, J. V. Hanna, P. R. Slater, J. Mater. Chem. 2012, 22, 8287-8293.

[157] Y. Zhu, W. Zhou, J. Sunarso, Y. Zhong, Z. Shao, Adv. Funct. Mater. 2016, 26, 5862-5872

[158] Wang, W., Xu, M., Xu, X., Zhou, W. and Shao, Z., 2020. Perovskite oxide based electrodes for high-performance photoelectrochemical water splitting. *Angewandte Chemie International Edition*, *59*(1), pp.136-152..

[159] Dresselhaus, M.S. and Dresselhaus, G., 1981. Intercalation compounds of graphite. *Advances in Physics*, *30*(2), pp.139-326.

[160] Suk, J.W., Piner, R.D., An, J. and Ruoff, R.S., 2010. Mechanical properties of monolayer graphene oxide. *ACS nano*, *4*(11), pp.6557-6564.

[161] Zhao, X.J., Hou, H., Fan, X.T., Wang, Y., Liu, Y.M., Tang, C., Liu, S.H., Ding, P.P., Cheng, J., Lin, D.H. and Wang, C., 2019. Molecular bilayer graphene. *Nature communications*, *10*(1), pp.1-7.

[162] Sun, H., Wu, L., Wei, W. and Qu, X., 2013. Recent advances in graphene quantum dots for sensing. *Materials today*, *16*(11), pp.433-442.

[163] Bacon, M., Bradley, S.J. and Nann, T., 2014. Graphene quantum dots. *Particle & Particle Systems Characterization*, *31*(4), pp.415-428.

[164] Li, Y., Zhao, Y., Cheng, H., Hu, Y., Shi, G., Dai, L. and Qu, L., 2012. Nitrogen-doped graphene quantum dots with oxygen-rich functional groups. *Journal of the American Chemical Society*, *134*(1), pp.15-18.

[165] Xu, Y., Liu, Y., Chen, H., Lin, X., Lin, S., Yu, B. and Luo, J., 2012. Ab initio study of energy-band modulation in graphene-based two-dimensional layered superlattices. *Journal of Materials Chemistry*, *22*(45), pp.23821-23829.

[166] Cao, X., Shi, Y., Shi, W., Lu, G., Huang, X., Yan, Q., Zhang, Q. and Zhang, H., 2011. Preparation of novel 3D graphene networks for supercapacitor applications. *small*, *7*(22), pp.3163-3168.

[167] Dimitrakakis, G.K., Tylianakis, E. and Froudakis, G.E., 2008. Pillared graphene: a new 3-D network nanostructure for enhanced hydrogen storage. Nano letters, 8(10), pp.3166-3170.

[168] Rasheed, M., Shihab, S. and Sabah, O.W., 2021, March. An investigation of the Structural, Electrical and Optical Properties of Graphene-Oxide Thin Films Using Different Solvents. In *Journal of Physics: Conference Series* (Vol. 1795, No. 1, p. 012052). IOP Publishing.

[169] Ren, H., Zheng, L., Wang, G., Gao, X., Tan, Z., Shan, J., Cui, L., Li, K., Jian, M., Zhu, L. and Zhang, Y., 2019. Transfer-medium-free nanofiber-reinforced graphene film and applications in wearable transparent pressure sensors. *Acs Nano*, *13*(5), pp.5541-5548.

[170] Tan, Y.W., Zhang, Y., Bolotin, K., Zhao, Y., Adam, S., Hwang, E.H., Sarma, S.D., Stormer, H.L. and Kim, P., 2007. Measurement of scattering rate and minimum conductivity in graphene. Physical review letters, 99(24), p.246803.Vancouver

[171] Abergel, D.S.L., Apalkov, V., Berashevich, J., Ziegler, K. and Chakraborty, T., 2010. Properties of graphene: a theoretical perspective. *Advances in Physics*, *59*(4), pp.261-482.

[172] Neto, A.C., Guinea, F., Peres, N.M., Novoselov, K.S. and Geim, A.K., 2009. The electronic properties of graphene. *Reviews of modern physics*, *81*(1), p.109.

[173] CheapTubes: https://www.cheaptubes.com/graphene-synthesis-properties-and-applications/

[174] Zhu, Y., Murali, S., Cai, W., Li, X., Suk, J.W., Potts, J.R. and Ruoff, R.S., 2010. Graphene and graphene oxide: synthesis, properties, and applications. *Advanced materials*, *22*(35), pp.3906-3924.

[175] Kavitha, M.K. and Jaiswal, M., 2016. Graphene: A review of optical properties and photonic applications. *Asian journal of Physics*, *7*, pp.809-831.

[176] "Optical properties of graphene"- Falkovsky L. A., *Journal of Physics Conference Series*, **2008**

[177] P. Subramanyam, T. Vinodkumar, D. Nepak, M. Deepa and C. Subrahmanyam, *Catal. Today*, 2019, 325, 73–80.

[178] L. Sun, J. Sun, X. Yang, S. Bai, Y. Feng, R. Luo, D. Li and A. Chen, *Dalt. Trans*., 2019, 48, 16091–16098.

[179] X. Zhang, R. Wang, F. Li, Z. An, M. Pu and X. Xiang, *Ind. Eng. Chem. Res*., 2017, 56, 10711–10719.

[180] T. Soltani, A. Tayyebi and B. K. Lee, Appl. Surf. Sci., 2018, 448, 465–473.

[181] T. Soltani, A. Tayyebi and B. K. Lee, *Sol. Energy Mater. Sol. Cells*, 2018, 185, 325–332.

[182] X. Han, Y. Wei, J. Su and Y. Zhao, *ACS Sustain. Chem. Eng*., 2018, 6, 14695–14703.

[183] Q. Pan, K. Yang, G. Wang, D. Li, J. Sun, B. Yang, Z. Zou, W. Hu, K. Wen and H. Yang, *Chem. Eng. J*., 2019, 372, 399– 407.

[184] A. Kormányos, E. Kecsenovity, A. Honarfar, T. Pullerits and C. Janáky, *Adv. Funct. Mater*., 2020, 30, 2002124.

[185] Y. Hou, M. Qiu, T. Zhang, J. Ma, S. Liu, X. Zhuang, C. Yuan and X. Feng, *Adv. Mater*., 2017, 29, 1604480.

[186] M. P. Cardona, M. Li, W. Li, J. McCall, D. Wang, Y. Li and C. Yang, *Mater. Today Energy*, 2018, 8, 8–14.

[187] J. Xie, J. Chen and C. M. Li, *Int. J. Hydrogen Energy*, 2017, 42, 7158–7165.

[188] S. Amaral Carminati, A. do Nascimento Barbosa, A. Luiz Martins de Freitas, F. L. Freire, F. L. Souza and A. F. Nogueira, *J. Catal*., 2019, 372, 109–118.

[189] A. Kormányos, E. Kecsenovity, A. Honarfar, T. Pullerits and C. Janáky, *Adv. Funct. Mater*., 2020, 30, 2002124.

[190] L. Yu, Y. Zhang, J. He, H. Zhu, X. Zhou, M. Li, Q. Yang and F. Xu, *J. Alloys Compd*., 2018, 753, 601–606.

[191] L. Sang, L. Lei and C. Burda, *Nano-Micro Lett*., 2019, 11, 97.

[192] N. Ahmed, A. A. Farghali, W. M. A. El Rouby and N. K. Allam, *Int. J. Hydrogen Energy*, 2017, 42, 29131–29139.

[193] R. Azimirad, S. Safa, M. Ebrahimi, S. Yousefzadeh and A. Z. Moshfegh, *J. Alloys Compd*., 2017, 721, 36–44.

[194] A. Bayat and E. Saievar-Iranizad, *J. Alloys Compd*., 2018, 755, 192–198.

[195] Z. Zeng, T. Li, Y. B. Li, X. C. Dai, M. H. Huang, Y. He, G. Xiao and F. X. Xiao, *J. Mater. Chem. A*, 2018, 6, 24686–24692.

[196] M. H. Elbakkay, W. M. A. El Rouby, S. I. El-Dek and A. A. Farghali, *Appl. Surf. Sci*., 2018, 439, 1088–1102.

[197] H. S. Sajjadizadeh, E. K. Goharshadi and H. Ahmadzadeh, *Int. J. Hydrogen Energy*, 2020, 45, 123–134.

[198] Z. Zeng, F. X. Xiao, X. Gui, R. Wang, B. Liu and T. T. Yang Tan, *J. Mater. Chem. A*, 2016, 4, 16383–16393.

[199] S. B. A. Hamid, S. J. Teh, C. W. Lai, S. Perathoner and G. Centi, *J. Energy Chem*., 2017, 26, 302–308.

[200] M. Ghorbani, H. Abdizadeh, M. Taheri and M. R. Golobostanfard, *Int. J. Hydrogen Energy*, 2018, 43, 7754– 7763.

[201] L. Sun, Y. Wang, F. Raziq, Y. Qu, L. Bai and L. Jing, *Sci. Rep*., 2017, 7, 1303.

[202] M. G. Hosseini, P. Y. Sefidi, Z. Aydin and S. Kinayyigit, *Electrochim. Acta*, 2020, 333, 135475.

[203] Z. Zhao, L. Zheng, W. Hu and H. Zheng, *Electrochim. Acta*, 2018, 292, 322–330.

[204] J. Ke, H. Zhou, J. Liu, Z. Zhang, X. Duan and S. Wang, *J. Colloid Interface Sci*., 2019, 555, 413–422.

[205] U. Sim, J. Moon, J. Lee, J. An, H. Y. Ahn, D. J. Kim, I. Jo, C. Jeon, S. Han, B. H. Hong and K. T. Nam, *ACS Appl. Mater. Interfaces*, 2017, 9, 3570–3580.

[206] Y. Sim, J. John, J. Moon and U. Sim, *Appl. Sci*., 2018, 8, 2046.

[207] K. Alam, Y. Sim, J. H. Yu, J. Gnanaprakasam, H. Choi, Y. Chae, U. Sim and H. Cho, *Materials (Basel)*., 2020, 13, 12.

[208] C. P. Han, C. J. Chen, C. C. Hsu, A. Jena, H. Chang, N. C. Yeh, S. F. Hu and R. S. Liu, *Catal. Today*, 2019, 335, 395–401.

[209] J. Nong, W. Wei, X. Song, L. Tang, J. Yang, T. Sun, L. Yu, W. Luo, C. Li and D. Wei, *Surf. Coatings Technol.*, 2017, 320, 579–583.

[210] H. Bae, H. Rho, J. W. Min, Y. T. Lee, S. H. Lee, K. Fujii, H. J. Lee and J. S. Ha, *Appl. Surf. Sci.*, 2017, 422, 354–358.

[211] Elbakkay MH, El Rouby WMA, El-Dek SI, Farghali AA. *Appl Surf Sci* 2018; 439:1088-102.

[212] Fa J, Hn L, Z Z, Nm H, A P. Ceram Int 2014;40:15159-65.

[213] Xu Z, Yin M, Sun J, Ding G, Lu L, Chang P, et al. Nanotechnology 2016; 27:115401.

[214] Zhang X, Zhang B, Huang D, Yuan H, Wang M, Shen Y. Carbon 2014; 80:591-8.

[215] Ahmed N, Farghali AA, El Rouby WMA, Allam NK. Int J Hydrogen Energy 2017; 42:29131-9.

[216] Nguyen Van C, Thanh Hai N, Olejnicek J, Ksirova P, Kohout M, Dvorakova M, et al. Mater Lett 2018;213:109-13.

[217] Alves AK, Frantz ACS, Berutti FA. FlatChem 2018; 12:26-34.

[218] Tayebi M, Kolaei M, Tayyebi A, Masoumi Z, Belbasi Z, Lee BK. Sol Energy 2019; 190:185-94.

[219] Yoon K-Y, Lee J-S, Kim K, Bak CH, Kim S-I, Kim J-B, et al. ACS Appl Mater Interfaces 2014;6:22634-9.

[220] Wu Q, Zhao J, Liu K, Wang H, Sun Z, Li P, et al. Int J Hydrogen Energy 2015; 40:6763-70.

[221] Zhang K, Shi X, Kim JK, Lee JS, Park JH. Nanoscale 2013; 5:1939-44.

[222] Nasiri MA, Sangpour P, Yousefzadeh S, Bagheri M. J Environ Chem Eng 2019; 7:102999.

[223] Yusoff N, Kumar SV, Pandikumar A, Huang NM, Marlinda AR, An'amt MN. Ceram Int 2015; 41:5117-28.

[224] Yusoff N, Kumar SV, Pandikumar A, Huang NM, Marlinda AR, An'amt MN. Ceram Int 2015; 41:5117-28.

[225] Ghorbani M, Abdizadeh H, Taheri M, Golobostanfard MR. Int J Hydrogen Energy 2018; 43:7754-63.

[226] Tayebi M, Tayyebi A, Masoumi Z, Lee B-K. Appl Surf Sci 2020; 502:144189.

[227] Chandrasekaran S, Chung JS, Kim EJ, Hur SH. Chem Eng J 2016; 290:465-76.

[228] Ng YH, Iwase A, Kudo A, Amal R. J Phys Chem Lett 2010; 1:2607-12.

[229] Soltani T, Tayyebi A, Lee B-K. Sol Energy Mater Sol Cells 2018; 185:325-32.

[230] Elbakkay MH, El Rouby WMA, El-Dek SI, Farghali AA. Appl Surf Sci 2018; 439:1088-102

[231] Yusoff N, Kumar SV, Pandikumar A, Huang NM, Marlinda AR, An'amt MN. Ceram Int 2015; 41:5117-28.

[232] Hou T-F, Shanmugasundaram A, Hassan MA, Johar MA, Ryu S-W, Lee D-W. Int J Hydrogen Energy 2019; 44:19177-92.

[233] Subramanyam P, Vinodkumar T, Nepak D, Deepa M, Subrahmanyam C. Catal Today 2019; 325:73-80.

[234] Zhang Z, Gao C, Li Y, Han W, Fu W, He Y, et al. Nanomater Energy 2016; 30:892-9.

[235] Luo J, Li D, Yang Y, Liu H, Chen J, Wang H. J Alloys Compd 2016; 661:380-8.

[236] Zhao Z, Zheng L, Hu W, Zheng H. Electrochim Acta 2018; 292:322-30.

[237] Mohamed MM, Ibrahim I, Salama TM. Appl Catal Gen 2016; 524:182-91.

[238] Ranjan R, Kumar M, Sinha ASK. *Int J Hydrogen Energy* 2019; 44:16176-89.

[239] Yaw CS, Ng WC, Ruan Q, Tang J, Soh AK, Chong MN. J Alloys Compd 2020; 817:152721.

[240] Ning F, Shao M, Xu S, Fu Y, Zhang R, Wei M, et al. *Energy Environ Sci* 2016; 9:2633-43.

[241] K. Yoon, J. H. Lee, J. Kang, J. Kang, M. J. Moody, M. C. Hersam, L. J. Lauhon, *Nano Lett*. 2016, 16, 7370.

[242] Wen, X., Yang, X., Li, M., Bai, L. and Guan, J., 2019. Co/CoO_x nanoparticles inlaid onto nitrogen-doped carbon-graphene as a trifunctional electrocatalyst. *Electrochimica Acta*, *296*, pp.830-841.

[243] Metal-organic framework-derived core-shell-structured nitrogen-doped CoCx/FeCo@C hybrid supported by reduced graphene oxide sheets as high performance bifunctional electrocatalysts for ORR and OER Hengyi Fang, Taizhong Huang, Yue Sun, Baotao Kang, Dong Liang, Shuo Yao, Jiemei Yu, M. Mayilvel Dinesh, Si Wu, Jin Yong Lee, Shun Mao, Journal of Catalysis.

[244] Mtukula AC, Bo X, Guo L. Highly active non-precious metal electrocatalyst for the hydrogen evolution reaction based on nitrogen-doped graphene supported MoO2/WN/Mo2N. J Alloys Compd. 2017;692:614-621.

[245] Chen W-F, Schneider JM, Sasaki K. Tungsten carbide–nitride on graphene nanoplatelets as a durable hydrogen evolution electrocatalyst. ChemSusChem. 2014;7(9):2414.

[246] Yan H, Tian C, Wang L, et al. Phosphorus-modified tungsten nitride/reduced graphene oxide as a high-performance, non- noble-metal electrocatalyst for the hydrogen evolution reaction. Angew Chem Int Ed. 2015;54(21):6325-6329.

[247] Wu L, Wang X, Sun Y, Liu Y, Li J. Flawed MoO2 belts transformed from MoO3 on a graphene template for the hydrogen evolution reaction. Nanoscale. 2015;7(16):7040-7044.

[248] Imran M, Yousaf AB, Zaidi SJ, Fernandez C. Tungsten- molybdenum oxide nanowires/reduced graphene oxide nanocomposite with enhanced and durable performance for electrocatalytic hydrogen evolution reaction. Int J Hydrogen Energy. 2017;42(12):8130-8138.

[249] Xie X, Lin L, Liu R-Y, Jiang Y-F, Zhu Q, Xu A-W. The synergistic effect of metallic molybdenum dioxide nanoparticle decorated graphene as an active electrocatalyst for an enhanced hydrogen evolution reaction. J Mater Chem A. 2015; 3(15):8055-8061.

[250] Suryakanti Debata, Santanu Patra, Sanchari Banerjee, Rashmi Madhuri, Prashant K.Sharma, Controlled Hydrothermal Synthesis of Graphene Supported $NiCo_2O_4$ Coral-Like Nanostructures: An Efficient Electrocatalyst for Overall Water Splitting, *Applied Surface Science*.

[251] E. Umeshbabu, G. Rajeshkhanna, P. Justin, G.R. Rao, $NiCo_2O_4$/rGO hybrid nanostructures for efficient electrocatalytic oxygen evolution, *J Solid State Electrochem* 20 (2016) 2725–2736.

[252] S.K. Bikkarolla, P. Papakonstantinou, $CuCo_2O_4$ nanoparticles on nitrogenated graphene as highly efficient oxygen evolution catalyst, J. Power Sources 281 (2015) 243-251.

[253] Reduced Graphene Oxide Supported Nickel-Manganese-Cobalt Spinel Ternary Oxide Nanocomposites and Their Chemical-Converted Sulfide Nanocomposites as Efficient Electrocatalysts for Alkaline Water Splitting Ran Miao, Junkai He, Sanjubala Sahoo, Zhu Luo, Wei Zhong, Sheng-Yu Chen, Curtis Guild, Tahereh Jafari, Biswanath Dutta, Shaylin A. Cetegen, Mingchao Wang, S. Pamir Alpay, and Steven L. Suib ACS Catal., 2016.

[254] Y. Liu, X. Shang, W. Gao, B. Dong, X. Li, X. Li, J. Zhao, Y. Chai, Y. Liu and C. Liu, *J. Mater. Chem. A*, 2017.

[255] T.-W. Lin, C.-J. Liu, J.-Y. Lin, Facile synthesis of MoS_3/carbon nanotube nanocomposite with high catalytic activity toward hydrogen evolution reaction, *Applied Catalysis B, Environmental* (2010).

[256] Y. Wei, H. Du, J. Kong, X. Lu, L. Ke, X.W. Sun, Multi-walled Carbon Nanotubes Modified ZnO Nanorods: a Photoanode for Photoelectrochemical Cell, *Electrochimica Acta* (2014).

[257] Deepti Chaudhary, Simrjit Singh, V.D.Vankar, Neeraj Khare, ZnO nanoparticles decorated multi-walled carbon nanotubes for enhanced photocatalytic and photoelectrochemical water splitting, *Journal of Photochemistry and Photobiology A: Chemistry* (2017).

[258] Chen, Y., Li, J., Hong, Z., Shen, B., Lin, B., & Gao, B. (2014). Origin of the enhanced visible-light photocatalytic activity of CNT modified g-C_3N_4 for H_2 production. *Physical Chemistry Chemical Physics*, 16(17), 8106.

[259] Cheng, H., Su, Y.-Z., Kuang, P.-Y., Chen, G.-F., & Liu, Z.-Q. (2015). Hierarchical $NiCo_2O_4$ nanosheet-decorated carbon nanotubes towards highly efficient electrocatalyst for water oxidation. *Journal of Materials Chemistry A*, 3(38), 19314–19321.

[260] Li F., Li J., Lin X., Li X., Fang Y., Jiao L., … Li R. (2015). Designed synthesis of multi-walled carbon nanotubes@Cu@MoS_2 hybrid as advanced electrocatalyst for highly efficient hydrogen evolution reaction. *Journal of Power Sources*, 300, 301–308.

[261] Chen, X., Yu, Z., Li, W., Zhou, Z., Zhai, S., Chen, J., … Chen, Y. (2018). Ultrathin Nickel Boride Nanosheets Anchored on Functionalized Carbon Nanotubes as Bifunctional Electrocatalysts for Overall Water Splitting. *Journal of Materials Chemistry A*.

[262] Nassar, Ibrahim, S. Wu, L. Li, and X. Li, *ChemistrySelect*, (2018).

[263] D. García, M. Isabel, and R. Gómez, *ChemSusChem*, (2017).

ANNEXURE 1

Literature Review

Extensive literature survey was performed on "Carbon interfaced metal oxide nano-heterostructure" as photoelectrodes in photoelectrochemical water splitting. **Table A.1** and **Table A.2** summarizes "graphene based metal oxides" and "multiwalled carbon nanotubes (MWCNTs)" for the aforesaid applications. The parameters studied range from modification performed, preparation method, and electrochemical observations. This whole survey describes the beauty of the carbon interfaced metal oxides.

Table A.1: Graphene based metal oxides for PEC water splitting applications

S. No.	Modification	Photo-electrode	Preparation Method	PEC Observation	Ref.
1	Mo:$BiVO_4$/rGO	Photoanode	Doctor blading	Photocurrent density= 8.51 mA cm^{-2} at 1.23 V_{RHE} in 0.1 M Na_2SO_4	**[177]**
2	$BiVO_4$/rGO/LDH	Photoanode	Electrodeposition	Photocurrent density= 1.13 mA cm^{-2} at 1.23 V_{RHE} in KPi (pH 7)	**[178]**
3	$BiVO_4$/rGO/LDH	Photoanode	Hydrothermal	Photocurrent density= 2.13 mA cm^{-2} at 1.23 V_{RHE} in 0.1 M KPi	**[179]**
4	$BiVO_4$/rGO	Photoanode	Drop casting	Photocurrent density= 0.13 mA cm^{-2} at 0.8 $V_{Ag/AgCl}$ 0.1 M Na_2SO_4	**[180]**
5	$BiVO_4$/rGO	Photoanode	Drop casting	Photocurrent density= 0.55 mA cm^{-2} at 1.2 $V_{Ag/AgCl}$ 0.1 M Na_2SO_4	**[181]**
6	$BiVO_4$/rGO/NiFe	Photoanode	Spin coating	Photocurrent density= 1.3 mA cm^{-2} at 1.23 V_{RHE} in 0.5 M Na_2SO_4	**[182]**
7	$BiVO_4$/GQDs/Co-Pi	Photoanode	Electrophoresis	Photocurrent density= 3.01 mA cm^{-2} at 0.6 V_{RHE} in 0.1 M KPi	**[183]**
8	$BiVO_4$/LDH/pGO /$CoPO_3$	Photoanode	Spin coating	Photocurrent density= 4.45 mA cm^{-2} at 1.2 V_{RHE} in 1 M potassium borate	**[184]**
9	Co-N/Flexible exfoliated grahene/Fe_2O_3	Photoanode	Spin coating	Photocurrent density= 2.15 mA cm^{-2} at 1.23 V_{RHE} in 1 M KOH	**[185]**
10	Fe_2O_3/SLG	Photoanode	Chemical Vapor Deposition	Photocurrent density= 0.75 mA cm^{-2} at 1.23 V_{RHE} in 1 M NaOH	**[186]**

11	Fe_2O_3/rGO	Photoanode	Dip coating	Photocurrent density= 0.88 mA cm^{-2} at 1.23 V_{RHE} in 1 M NaOH	**[187]**
12	Fe_2O_3/SLG	Photoanode	Chemical Vapor Deposition	Photocurrent density= 1.64 mA cm^{-2} at 1.23 V_{RHE} in 1 M NaOH	**[188]**
13	FeNiOOH/Fe_2O_3/G	Photoanode	Spray-coating	Photocurrent density= 2 mA cm^{-2} at 1.45 V_{RHE} in 1 M NaOH	**[189]**
14	Fe_2O_3/rGO/Ag	Photoanode	Hydrothermal	Photocurrent density= 0.72 mA cm^{-2} at 1.23 V_{RHE} in 1 M KOH	**[190]**
15	Ag-TiO_2/rGO	Photoanode	Anodization	Photocurrent density= 0.98 mA cm^{-2} at 1 $V_{Ag/AgCl}$ in 0.5 M Na_2SO_4	**[191]**
16	TiO_2-rGO	Photoanode	Drop casting	Photocurrent density= 1.44 mA cm^{-2} at 1 $V_{Ag/AgCl}$ in 1 M KOH	**[192]**
17	TiO_2/GQDs	Photoanode	Spin coating	Photocurrent density= 6.35 mA cm^{-2} at 0.5 $V_{Ag/AgCl}$ in 0.1 M Na_2S	**[193]**
18	TiO_2/SNGQDs	Photoanode	Spin coating	Photocurrent density= 0.85 mA cm^{-2} at 0.5 $V_{Ag/AgCl}$ in 0.1 M Na_2SO_4	**[194]**
19	TiO_2@Ag/GQDs	Photoanode	Layer-by-layer	Photocurrent density= 0.6 mA cm^{-2} at 1 $V_{Ag/AgCl}$ in 0.5 M Na_2SO_4	**[195]**
20	S-TiO_2/S-doped rGO	Photoanode		Photocurrent density= 3.36 mA cm^{-2} at 1 $V_{Ag/AgCl}$ in 1 M KOH	**[196]**
21	TiO_2/GQDs	Photoanode	Spin coating	Photocurrent density= 0.26 mA cm^{-2} in 0.5 M KOH	**[197]**
22	ZnO NWs/N-doped GQDs	Photoanode	Layer-by-layer	Photocurrent density= 0.6 mA cm^{-2} at 1 $V_{Ag/AgCl}$ in 0.5 M Na_2SO_4	**[198]**
23	ZnO/rGO	Photoanode	Electrochemical reduction	Photocurrent density= 1.8 mA cm^{-2} at 0.7 $V_{Ag/AgCl}$ in 1 M KOH	**[199]**
24	ZnO/rGO	Photoanode	Sol-gel dip coating	Photocurrent density= 1.02 mA cm^{-2} at 1.5 $V_{Ag/AgCl}$ in 0.5 M Na_2SO_4	**[200]**
25	WO_3/rGO	Photoanode	Doctor blading	Photocurrent density= 2.85 mA cm^{-2} at 0.6 $V_{Ag/AgCl}$ in 0.5 M Na_2SO_4	**[201]**
26	CSA-PANI-WO_3/rGO	Photoanode	Spin coating	Photocurrent density= 1.54 mA cm^{-2} at 1.23 V_{RHE} in 0.1 M Na_2SO_4	**[202]**
27	WO_3/Silane/GO	Photoanode	Dip coating	Photocurrent density= 1.25 mA cm^{-2} at 1.23 V_{RHE} in 0.5 M Na_2SO_4	**[203]**
28	WO_3/rGO	Photoanode	Hydrothermal	Photocurrent density= 750 nA cm^{-2} at 0 V_{SCE} in 0.05 M Na_2SO_4	**[204]**

29	Si/double layer G	Photocathode	• Chemical Vapor Deposition • Layer by Layer • Plasma treatment	• Photocurrent density= -30 mA cm^{-2} at -0.7 V_{RHE} in 1 M $HClO_4$ • Onset Potential= 0.2 V_{RHE} • Source: 300 W Xe arc lamp (AM 1.5G, 100 mW cm^{-2})	**[205]**
30	Si NWs/rGO	Photocathode	Metal-Catalysed Electroless Chemical Etching	• Photocurrent density= -23.1 mA cm^{-2} at 0 V_{RHE} in 1 M $HClO_4$ • Onset Potential= 0.33 V_{RHE} • Source: 300 W Xe arc lamp (AM 1.5G, 100 mW cm^{-2})	**[206]**
31	Si/hydrophobic rGO	Photocathode	Atmospheric Plasma Chemical Vapor Deposition	• Photocurrent density= -3.3 mA cm^{-2} at -0.6 V_{RHE} in 1 M $HClO_4$ • Onset Potential= -0.15 V_{RHE} • Source: 300 W Xe arc lamp (AM 1.5G, 100 mW cm^{-2})	**[207]**
32	Si/multi-layer G	Photocathode	Atmospheric Pressure Chemical Vapor Deposition	• Photocurrent density= -28.3 mA cm^{-2} at -0.385 V_{RHE} in 1 M $HClO_4$ • Onset Potential= -0.36 V_{RHE} • Source: 300 W Xe arc lamp (AM 1.5G, 100 mW cm^{-2})	**[208]**
33	Si/GNWs/CdTe	Photoanode	• Radio Frequency Plasma enhanced Chemical Vapor Deposition • Vapor Transport Deposition	• Photocurrent density= 3 mA cm^{-2} at 0 V_{RHE} in 0.5 M Na_2S • Source: 500 W Xe arc lamp (100 mW cm^{-2})	**[209]**
34	Si/Gr/GaN NWs	Photoanode	• Chemical Vapor Deposition • Molecular Beam Epitaxy	• Photocurrent density= 0.24 mA cm^{-2} at 0 $V_{Ag/AgCl}$ in 1 M NaOH • Source: 500 W Xe arc lamp (100 mW cm^{-2})	**[210]**
35	rGO-TiO_2		Solvothermal	• Photocurrent density= 1.65 mA cm^{-2} at 1 $V_{Ag/AgCl}$ in 1 M KOH	**[211]**
36	rGO-TiO_2		Dip-coating	• Photocurrent density= 80.2 µA cm^{-2} in 0.5 M Na_2SO_4	**[212]**
37	Graphene QDs-TiO_2		Electrophoresis deposition	• Photocurrent density= 2.92 mA cm^{-2} at 0 $V_{Ag/AgCl}$ in 1 M KOH	**[213]**

				• IPCE= 72% at 370 nm • Donor Density= 1.7 X 10^{18} cm^{-3}	
38	ERGO-TiO_2		Electrochemical reduction	• Photocurrent density= 1.44 mA cm^{-2} at 1.23 V_{RHE} in 1 M KOH • IPCE= 8.14% at 400 nm • Donor Density= 6 X 10^{20} cm^{-3}	**[214]**
39	Graphene-TiO_2		Solvothermal	• Photocurrent density= 1.449 mA cm^{-2} at V_{RHE} in 1 M KOH	**[215]**
40	Graphene-TiO_2		Magnetron sputtering	• Photocurrent density= 24 µA cm^{-2} at 0.3 $V_{Ag/AgCl}$ in 1 M Na_2SO_4	**[216]**
41	Graphene-TiO_2 QDs		Microwave-assisted Oleothermal	• Photocurrent density= 0.8 mA cm^{-2} at 1.23 V_{RHE} in 0.1 M KOH	**[217]**
42	rGO-TiO_2		Hydrothermal	• Donor Density= 9.64 X 10^{25} cm^{-3} in 1 M KOH	**[218]**
43	Graphene Inverse Opal - α-Fe_2O_3		Hydrothermal	• Photocurrent density= 1.62 mA cm^{-2} at 1.5 V_{RHE} in 1 M KOH • IPCE= 42% at 320 nm	**[219]**
44	rGO-Fe_2O_3		Spin coating	• Photocurrent density= 0.63 mA cm^{-2} at 1.5 V_{RHE} in 1 M KOH • IPCE= 18.6% at 400 nm	**[220]**
45	Graphene- α Fe_2O_3		Template assisted electro-deposition	• Photocurrent density= 3 mA cm^{-2} at 0.5 $V_{Ag/AgCl}$ in 1 M KOH	**[221]**
46	rGO-α Fe_2O_3		Electrodeposition	• Photocurrent density= 0.98 mA cm^{-2} at 0.23 $V_{Ag/AgCl}$ in 1 M KOH	**[222]**
47	rGO-Fe_3O_4		Hydrothermal	• Photocurrent density= 280 µA cm^{-2} at 1.23 V_{RHE} in 0.1 M KOH	**[223]**
48	rGO-ZnO		Hydrothermal	• Photocurrent density= 430 µA cm^{-2} at 1.23 V_{RHE} in 0.1 M KOH	**[224]**
49	rGO-ZnO		Sol-gel	• Photocurrent density= 1.04 mA cm^{-2} at 1.5 $V_{Ag/AgCl}$ in 0.5 M Na_2SO_4	**[225]**
50	rGO-ZnO		Wet Chemical	• Photocurrent density= 0.6 mA cm^{-2} at 0.6 $V_{Ag/AgCl}$ in 0.5 M Na_2SO_4	**[226]**

				• Donor Density= 2.93 X 10^{26} cm^{-3}	
51	GO-ZnO		Hydrothermal	• Photocurrent density= 1.517 mA cm^{-2} at 1.45 V_{RHE} in 1 M NaOH • IPCE= 10.41% at 360 nm	**[227]**
52	rGO-$BiVO_4$		Single-step Photocatalytic Reaction	• Photocurrent density= 70 µA cm^{-2} at 1.45 V_{RHE} in 0.1 M Na_2SO_4 • IPCE= 4.2% at 400 nm	**[228]**
53	rGO-$BiVO_4$		Visible-light-assisted photocatalytic reduction	• Photocurrent density= 554.4 µA cm^{-2} at 1.2 $V_{Ag/AgCl}$ in 0.1 M Na_2SO_4 • IPCE= 4.5% at 300 nm • Donor Density= 7.52 X 10^{16} cm^{-3}	**[229]**
54	S-TiO_2/S-rGO		Solvothermal	• Photocurrent density= 3.36 mA cm^{-2} at 1 $V_{Ag/AgCl}$ in 1 M KOH	**[230]**
55	rGO/Fe_3O_4-ZnO		Hydrothermal	• Photocurrent density= 850 µA cm^{-2} at 1.23 V_{RHE} in 0.1 M KOH • Donor Density= 9.36 X 10^{20} cm^{-3}	**[231]**
56	Mo-$BiVO_4$/rGO		Wet impregnation method	• Photocurrent density= 8.51 mA cm^{-2} at 1.23 V_{RHE} in 0.1 M Na_2SO_4 • IPCE= 25% at 420 nm	**[232]**
57	rGO/ITO-Fe_2O_3		Electrodeposition	• Photocurrent density= 5.38 mA cm^{-2} at 0.6 V_{SCE} in 1 M NaOH • IPCE= 33% at 390 nm	**[233]**
58	Au/rGO/Hydrogenated titanium dioxide nanotube		Electrophoretical deposition	• Photocurrent density= 224 µA cm^{-2} in 1 M KOH • IPCE= 5.8% at 580 nm	**[234]**
59	WO_3nanosheets/Silane/GO		Chemical bath deposition	• Photocurrent density= 1.25 mA cm^{-2} at 1.23 V_{RHE} in 0.5 M Na_2SO_4 • Donor Density= 8.7 X 10^{23} cm^{-3} • IPCE= 41.5% at 380 nm	**[235]**
60	ZnO-Cu_2O/rGO		Electrodeposition	• Photocurrent density= 10.11 mA cm^{-2} at 1.23 V_{RHE} in 0.5 M Na_2SO_4	**[236]**

				• IPCE= 73.53% at 350 nm	
61	$MnFe_2O_4$/GO		Sol gel-hydrothermal	• Photocurrent density= 0.875 mA cm^{-2} at 1.23 V_{RHE} in 0.2 M Na_2SO_3 and 0.1 M phosphate buffer solution (pH 6.9) • IPCE=29%	**[237]**
62	MoS_2-CdS/rGO		Hydrothermal	Photocurrent density= 20.2 mA cm^{-2} at -0.6 V_{SHE} in 0.35 M Na_2SO_3 and 0.25 M Na_2S	**[238]**
63	V_2O_5/rGO/$BiVO_4$		Electrodeposition	Photocurrent density= 2.1 mA cm^{-2} at 1.5 $V_{Ag/AgCl}$ in 0.5 M Na_2SO_4	**[239]**
64	TiO_2/Graphene/Ni Fe-layered double hydroxide		Spin-coating and Electrodeposition	• Photocurrent density= 9.74 mA cm^{-2} at 0.6 V_{SCE} in 0.5 M Na_2SO_4 • Donor Density= 3.32 X 10^{19} cm^{-3} • IPCE= 5.12% at 400 nm	**[240]**
65	Si/CNTs/graphene		Film transfer	• Photocurrent density= 8 mA cm^{-2} at 1.83 V in 1 M KOH • Onset Potential = 1.4 V • Source: 1-sun illumination (AM 1.5G) 100 mW cm^{-2}	**[241]**
66	Co@NC-G-700		Co/CoO_x nanoparticles embedded onto N-doped C-graphene obtained by the pyrolysis of GO (which is synthesized by modified Hummers method) supported cobalt ZIF-67 under a N_2 atmosphere.	• Photocurrent Density= 10 mA cm^{-2} in 1 M KOH • E_{onset} (V_{RHE}) = 0.93 V in 0.1 M KOH • $E_{Half\text{-}wave}$ (V_{RHE}) = 0.83 V in 0.1 M KOH • Overpotential = 322 mV in 1 M KOH • Overpotential = 140 mV in 0.5 M H_2SO_4 • Tafel slope = 73.7 mV dec^{-1} in 1 M KOH • Tafel slope = 62 mV dec^{-1} in 0.5 M H_2SO_4 • E_{onset} (V_{RHE}) = 0.93 V in 0.1 M KOH • $E_{Half\text{-}wave}$ (V_{RHE}) = 0.83 V in 0.1 M KOH • Surface Composition ○ C = 91.7 mol% ○ O = 4.5 mol%	**[242]**

				○ Co = 1.2 mol% ○ Co = 6.1 wt % ○ Total N_2 = 2.6% ○ Pyridinic-N = 55.1% ○ Co-N_x = 12.1 ○ Pyrrolic-N = 12.1% ○ Graphitic-N = 20.7% • The surface Co-N_x, Co-O-Co, Co-N-C and Co-O-C sites might work together in OER.	
67	Core-shell-structured nitrogen-doped CoC_x/FeCo@C/reduced graphene oxide (rGO) hybrid, which is derived from Fe-doped $Co3[Co(CN)_6]_2$ MOFs		GO by a modified Hummers' method	• Current intensity = 10 mA cm^{-2} • Onset Potential = 1.0183 V_{RHE} • Half-Wave Potential = 0.9653 V_{RHE} • Peak Current Intensity 0.9233 mA cm^{-2} • Overpotential = 390 mV • Large surface area • Stable anchoring sites	**[243]**
68	Nitrogen-doped graphene (NGR) supported MoO_2/ MoW nitride alloy (MoWON/NGR)			• Photocurrent Density= 10 mA cm^{-2} in 0.5 M H_2SO_4 • Onset Potential= 120 mV (vs. RHE) • Tafel slope = 84 mV dec^{-1} • Stability= 40,000 seconds, 2000 CV	**[244]**
69	Tungsten Carbide–Nitride on Graphene Nanoplatelets (W_2C-WN/GnP)			• Photocurrent Density= 10 mA cm^{-2} in 0.1 M $HClO_4$ • Over Potential = 120 mV (vs. RHE) • Stability= 300 hours	**[245]**
70	Phosphorus-modified tungsten nitride/reduced graphene oxide (P-WN/rGO)			• Photocurrent Density= 10 mA cm^{-2} in 0.5 M H_2SO_4 • Over Potential = 85 mV (vs. RHE) • Tafel slope = 54 mV dec^{-1} • Stability = 20 hours, 5000 CV	**[246]**

71	MoO_3/Graphene			• Over Potential = -0.16 V (vs. RHE) in 0.5 M H_2SO_4 • Tafel slope = 58 mV dec^{-1} • Stability = 1000 CV	**[247]**
72	W-Mo-O/rGO			• Over Potential = 50 mV (vs. RHE) in 0.1 M $HClO_4$ • Tafel slope = 46 mV dec^{-1} • Stability = 1000 CV	**[248].**
73	MoO_2/rGO			• Photocurrent Density= 10 mA cm^{-2} in 0.5 M H_2SO_4 • Over Potential = 190 mV (vs. RHE) • Tafel slope = 49 mV dec^{-1} • Stability = 1000 CV	**[249]**
74	rGO-$NiCo_2O_4$ nanocorals		Hydrothermal	❖ **<u>OER</u>** • Photocurrent Density = 1550 mA cm^{-2} • Onset Potential = 0.508 V (vs Ag/AgCl) • Onset Potential = 1.55 V (vs RHE) • Over Potential = 0.048 V (vs Ag/AgCl) at 10 mA cm^{-2} • Over Potential = 0.057 V (vs RHE) at 10 mA cm^{-2} • Tafel Slope = 46.74 mV $decade^{-1}$ ❖ **<u>HER</u>** • Photocurrent Density = -600 mA cm^{-2} • Onset Potential = -1.22 V (vs Ag/AgCl) • Onset Potential = -0.173 V (vs RHE) • Over Potential = 0.144 V (vs Ag/AgCl) at 10 mA cm^{-2} • Over Potential = 0.319 V (vs RHE) at 10 mA cm^{-2} • Tafel Slope = 90.63 mV $decade^{-1}$	**[250]**
75	$NiCo_2O_4$/rGO nanonet		Solvothermal	• Photocurrent Density= 10 mA cm^{-2}	**[251]**

				• Onset Potential = 1.57 V (vs RHE) • Over Potential = 0.450 V (vs RHE) • Tafel Slope = 53 mV decade^{-1}	
	$NiCo_2O_4$/rGO microsphere			• Photocurrent Density= 10 mA cm^{-2} • Onset Potential = 1.57 V (vs RHE) • Over Potential = 0.510 V (vs RHE) • Tafel Slope = 62 mV decade^{-1}	
76	$CuCo_2O_4$/NrGO		Solvothermal	• Photocurrent Density= 10 mA cm^{-2} • Over Potential = 0.360 V (vs Ag/AgCl) • Tafel Slope = 64 mV decade^{-1}	**[252]**
77	Spinel Ternary Oxide Material Consisting of Nickel, Manganese, and Cobalt supported on Reduced Graphene Oxide (rGO/NMC-312 oxide)	rGO/NMC-312 oxide= Anode rGO/NMC-312 sulfide= Cathode	• GO = modified Hummer's method • rGO/NMC Ternary Oxide Composites = Two-Step Solvothermal Method • Direct conversion of rGO/NMC-312-O into rGO/NMC-312-S by gaseous sulfurization protocol using a laboratory scale sulfurization apparatus	• 1.56 V is required to achieve a current density of 20 mA cm^{-2} in an alkaline medium at room temperature • Tafel slope = 52 mV decade^{-1} • Stability = 24 hours • Overpotential at current density of 10 mA cm^{-2} ○ rGO/NMC-312-O = 320 mV ○ rGO/NMC-312-S = 151 mV • Charge Transfer Resistance ○ rGO/NMC-312-S = 29 Ω ○ rGO/NMC-312-O = 47 Ω • Due to suitable energetics	**[253]**
78	$CoMoS/CoMoO_4$ shell-core nanorods supported on N-doped reduced graphene oxide (NRGO)		• GO by modified Hummers method	• Overpoential = 80 mV • Tafel slope = 58 mV decade^{-1} • Exchange current density = 428 µA cm^{-2} • Stability = 1000 cycles	**[254]**

				• Due to high dispersion and availability of the active sites of CoMoS active phase for HER on the surface of NRGO with high surface area and good electrical conductivity	

Table A.2: Application of MWCNTs for PEC water splitting

S. No.	Photoelectrode	Preparation Method	Role of MWCNT	PEC Observation	Explanation Given	Ref.
1	MoS_3/CNT (Actual catalyst is amorphous MoS_2)	Wet Chemistry Process	Provided sites for high dispersion of amorphous MoS_3 for electrochemically reducing to amorphous MoS_2 nanoparticles on MWCNT surface with higher number of exposed edges.	• Optimal loading of MoS_3 on MWCNTs= 33 wt.% • Current Density= 173 micro A cm^{-2} • Overpotential=0.13 V • Tafel slope=40 mV/decade • Stability=500 cycles (88% decrement)	High HER activity of nanocomposite was correlated to amorphous MoS_3 morphology on conductive CNTs	**[255]**
2	MWCNTs modified ZnO nanorods	Hydrothermal Method followed by simple solution deposition	Self-anchored MWCNTs on ZnO nanorods acted as a hole-attracting phase	• Photo Current Conversion efficiency= 0.646 % (2.1 times higher than pristine ZnO nanorods) • J_{sc} = 0.25 mA cm^{-2} (4 times higher than pristine ZnO nanorods) • PCE = 0.646 % (2.16 times higher than pristine ZnO nanorods) • Photocurrent density shows a trend of increase followed by decrease along with the increase of the loading of MWCNTs.	Increased light absorption from rougher surface and effective charge carrier transport from conductive MWCNTs Reduction of the recombination rate of electrons and holes due to the electronic properties and bridge function of incorporated MWCNTs	**[256]**

				• Optimized concentration of MWCNTs/ethanol suspension = 0.002 wt%		
3	ZnO/MWCNT	• MWCNT: Thermal Chemical Vapor Deposition method • ZnO/MWCNT nanocomposite: Sol-Gel Method	Photogenerated charge carrier separation	• Photocurrent density= 1.14 mA cm^{-2} (~5 times higher than bare ZnO) • V_{FB} value= -0.25 V vs. Ag/AgCl • $N_d = 2 \times 1019\ cm^{-3}$	Decrease in band-bending and effective interfacial electron transfer due conducting CNT scaffold facilitated the charge collection and charge transport	**[257]**
4	MWCNT/g-C_3N_4	• Pure g-C_3N_4 prepared using cyanamide as precursor. • CNT was surface-functionalized by a HNO_3-steaming procedure.	MWCNT improved electron–hole separation on the excited g-C_3N_4 by prolonging the lifetimes of charge carriers and improving the population distribution of short-lived and long-lived charge carriers.	• Optimal CNT content is found to be 0.2 wt.% in the composite • H_2 production rate of 39.4 mmol h^{-1} • 2.4 fold enhancement in efficiency	Enhanced charge-transfer effect due to the intimate interactions between g-C_3N_4 and conjugated CNT.	**[258]**
5	$NiCo_2O_4$ /CNTs	Spinel $NiCo_2O_4$ nanosheets grown on the mildly oxidized MWCNTs via a simple one-pot solution method	• Remarkable conductivity • Large specific surface area	• Current Density= 83 mA cm^{-2} at 0.7 V • Tafel slope of $NiCo_2O_4$ /CNTs= 68.1 mV dec^{-1} • Stability= 10 hours (83%) • Charge transfer resistance= 6.9 Ω • BET specific surface area=170 $m^2\ g^{-1}$ • Pore volume= 0.7 $cm^3\ g^{-1}$ • Highly coulombic efficiency for the OER process	Synergistic effect between the oxygen-enriched group and metal ions	**[259]**

6	MWCNTs @Cu@MoS_2	• Chemical Process • Hydrothermal Method	MWCNTs and Cu nanoparticles improved the electrical conductivity	• Photocurrent density= 10 mA cm^{-2} • Overpotential=184 mV • Tafel slope= 62 mV per decade • Stability= 1000 cycles	Enhanced catalytic activity by synergistic effect of MWCNT @ Cu with edge-exposed MoS_2 coating	**[260]**
7	Ni_xB/f-MWCNT	f-MWCNT anchored the ultrathin nickel boride (Ni_xB) sheets on its surface	MWCNTs prepared by modified Hummers method	• Photocurrent density= 10 mA cm^{-2} at 1.6 V • Overpotentials = 286 or 116 mV • Electrochemically active surface area=3.4 times of the Ni_xB • Tafel slope = 70.4 mV dec^{-1} • Charge transfer resistance= 24.2 Ω • Chronopotentiometric decay at 20 mA cm^{-2} is negligible after 100 test hours • Follows the Volmer–Heyrovsky mechanism • Water discharge (Volmer) reaction is the rate-limiting step	In situ formation of highly active NiOOH/Ni_xB and $Ni(OH)_2$/Ni_xB heterojunctions	**[261]**